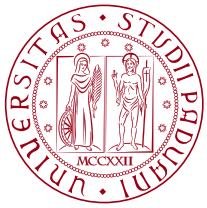

UNIVERSITÀ
DEGLI STUDI
DI PADOVA

DEPARTMENT OF
INFORMATION
ENGINEERING
UNIVERSITY OF PADOVA

Master Thesis *in* Control Systems Engineering

Development *of* a pure pursuit lane keeping controller *for* a 1:10 scale autonomous vehicle

Master Candidate Antonio Gallina
2021441

Supervisor Prof. Mattia Bruschetta

Academic Year 2021/2022
October 10, 2022

Beautiful is better than ugly.
Explicit is better than implicit.
Simple is better than complex.
Complex is better than complicated.
Flat is better than nested.
Sparse is better than dense.
Readability counts.
Special cases aren't special enough to break the rules.
Although practicality beats purity.
Errors should never pass silently.
Unless explicitly silenced.
In the face of ambiguity, refuse the temptation to guess.
There should be one – and preferably only one – obvious way to do it.
Although that way may not be obvious at first unless you're Dutch.
Now is better than never.
*Although never is often better than *right* now.*
If the implementation is hard to explain, it's a bad idea.
If the implementation is easy to explain, it may be a good idea.
Namespaces are one honking great idea – let's do more of those!

Tim Peters

Abstract

Research on Autonomous Vehicles (AVs) has experienced an increasingly significant growth of interest in the last few years because of its potential to enhance safety, efficiency and convenience of automotive transportation. Anyway, due to its complexity, there are still a lot of technical and social challenges to be tackled in this field.
The driving task of an AV can be grouped mainly into five parts: Sensing & Input, Perception & Scene Understanding, Behavior Planning & Selection, Motion & Control and Actuation. Path Tracking Controllers (PTCs) lay in the Motion layer and play a key role in controlling the lateral and longitudinal dynamics of the vehicle by generating suitable control signals for the low-level actuation part, in order to follow the planned path.
This thesis stems from the participation of the DEI-Unipd Team in the Bosch Future Mobility Challenge 2022 and focuses on the development of a lane keeping PTC for a 1:10 scale vehicle: lateral control is based on the traditional Pure Pursuit strategy and longitudinal control is obtained by means of a PID controller with a variable velocity reference. In this scenario, the Lookahead Heading Error (LHE) — input to the PP-based controller — is computed by means of a Convolutional Neural Network (CNN) which is trained by means of a Gazebo simulator: virtual augmented images taken from a perturbed path are used in a supervised strategy to characterize the LHE. Throughout this thesis the LHE will be assumed to be available at a fixed distance.
A pure camera based controller is then proposed, specifically addressing the effects of the delay in the steering actuation mechanism and the "corner-cutting" effect, characteristic of the Pure Pursuit strategy. Thanks to a low-noise input provided by the CNN, a derivative action and a velocity reference generation technique, uncommon in PP-type approaches, were introduced in order to cope with the presence of limited steering dynamics and constraints imposed by the LHE estimation.

Contents

List of Figures

CHAPTER

1 Introduction

Research on Autonomous Vehicles (AVs) has experienced an increasingly significant growth of interest in the last few years because of its potential to enhance safety, efficiency and convenience of automotive transportation. Anyway, due to its complexity, there are still a lot of technical and social challenges to be tackled in this field. The driving task of an AV can be grouped mainly into five parts: Sensing & Input, Perception & Scene Understanding, Behavior Planning & Selection, Motion & Control and Actuation. Path Tracking Controllers (PTCs) lay in the Motion layer and play a key role in controlling the lateral and longitudinal dynamics of the vehicle by generating suitable control signals for the low-level actuation part, in order to follow the planned path.

This thesis stems from the participation of the DEI-Unipd Team in the Bosch Future Mobility Challenge 2022 and focuses on the development of a lane keeping PTC for a 1:10 scale vehicle: lateral control is based on the traditional Pure Pursuit strategy and longitudinal control is obtained by means of a PID controller with a variable velocity reference.

The Pure Pursuit strategy is a nonlinear kinematic proportional path tracking control strategy that relies on the Ackerman geometry of a rear wheel driving bicycle model to define a point on the reference path ahead of the vehicle by a distance L_d, called the *lookahead distance*. Besides the

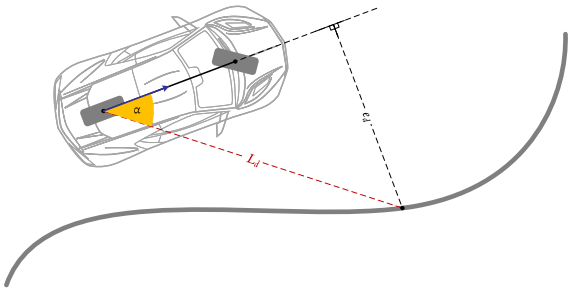

Figure 1.1: Relevant parameters of the PP strategy

lookahead distance, which is the only tunable parameter, other key PP parameters are illustrated in Fig.1.1. The angle the car heading direction forms with the line joining the rear axis and the lookahead point on the path will be called hereinafter *Lookahead Heading Error* (LHE) and denoted with the letter α. The cross track error between the point on the path and the heading direction of the vehicle, denoted with the symbol e_d, will be referred to as *Lookahead Lateral Error* (LLE).

1.1 Scope and delimitations of the thesis

The aim of this thesis is developing a lane keeping PP controller in a limited scenario that possibly maximizes velocity along with tracking performance. The 1:10 scale vehicle is equipped with a cheap DC servomotor for steering actuation with slow dynamics and a cheap steering transmission that, besides introducing slack in steering maneuvers, sets a bound on the commanded steering angle. The reference track is composed of both straight sections and circular arcs with different radii and is characterized by a fixed width that sets a bound on the lateral motion. The heading motion is also bounded due to the usage of a camera with a limited FoV for estimating the the Lookahead Heading Error (LHE). The LHE - input to the PP-based controller — is computed by means of a Convolutional Neural Network (CNN) which is trained by means of a Gazebo simulator where virtual augmented images taken from a perturbed path are used in a supervised strategy to characterize the LHE. Throughout this thesis the LHE will be assumed to be available at a fixed distance.

1.2 Literature review on PP control

The field of automatic steering control is fairly well established and a lot of different methods from linear PID control to optimization based MPC can be implemented for tracking a given path [15, 19, 28]. Among PTCs, the PP controller lies in the subset of geometric controllers, i.e. controllers that rely on the steering geometry of the vehicle, usually regardless of dynamic effects.

The Pure Pursuit (PP) control strategy can be dated back in time to 1969, when Scharf et al. in [20] introduced it for guiding missiles towards a nonmaneuvering target [12]. The first discussion on PP control in the robotic field appeared in [24], where Wallace et al. discussed a visual servoing based control scheme for path tracking. Based on this, Amidi et al. in [2] implemented and tested such technique for an autonomous vehicle and Coulter in [5] discussed in detail the implementation of the PP algorithm, its geometric derivation and some insights into its performance as a function of its parameters.

Since then, due to the remarkable simplicity of its implementation, easily tunable parameters and low computational cost, the PP controller has been widely studied by researchers and implemented successfully in many applications for path tracking, both for indoor and for outdoor ground vehicles including the DARPA Urban Challenge [3, 4], as well as for trajectory tracking of unmanned air vehicles [17].

In [13] Murphy discussed stability conditions in the presence of actuation delay by adopting a transfer function approach in the case of straight road. The major contribution to stability analysis of the PP controller in the presence of delay was given by Ollero and Heredia in [14], both for straight and for constant curvature paths, taking into account steering dynamics and static delay. A thorough search of the relevant literature yielded only one article related to the proposed PP control law with derivative contribution. In 2022, Wang et al. in [26] introduced an improved pure pursuit control law based on a heading error rate. The velocity reference generation law is discussed in [7], although no reference related to the proposed Ackerman-based technique has been found.

1.3 Structure of the thesis

In this thesis a pure camera based controller is proposed, specifically addressing the effects of the delay in the steering actuation mechanism and the "corner-cutting" effect, characteristic of the Pure Pursuit strategy. In Chapter 2, starting from the global nonlinear single track vehicle model, a local model in path coordinates is presented along with a model for the steering actuator. Based on the local bicycle model, two models for control are then derived both in the straight and in the circular path scenarios. The Pure Pursuit controller is widely discussed in Chapter 3: besides its geometric derivation and implementation issues, particular attention is paid to the stability study of the closed loop control system in the delay free straight and circular scenarios. Thanks to a low-noise input provided by the CNN, a derivative action and a velocity reference generation technique, uncommon in PP-type approaches, are introduced in order to cope with the presence of limited steering dynamics and constraints imposed by the LHE estimation.
In Chapter 4 stability of the linearized closed loop control system in both scenarios is investigated in the presence of both steering dynamics and static delay resorting to time-delay stability theory. Eventually in Chapter 5, results from testing the proposed control law in a laboratory environment are discussed and compared by means of suitable performance metrics.
Before going into further details, it is worth to mention that the idea behind this lane keeping controller lead the DEI-Unipd Team to win the BFMC speed challenge and, as a part of other AD algorithms, helped to to win the 1st prize in the BFMC 2022.

Figure 1.2: Photos from the Bosch Future Mobility Challenge 2022: (A) Finalist teams (B) DEI-Unipd Team (C) DEI-Unipd car during finals

CHAPTER

2 System modelling

Models used for PP stability analysis are derived in this Chapter.

Specifically addressing a PP control strategy, a model of the vehicle is derived irrespective of dynamic components of the vehicle. The Ackerman geometry, described in Sec.2.1, holds in this scenario and the four wheel vehicle can be approximated by a single track kinematic vehicle model. A global bicycle model is then derived in Sec.2.2 under the assumption that the wheels are purely rolling without any side slip.

In view of a path tracking type of control, a local bicycle model in path coordinates is derived in Sec.2.3 highlighting the evolution of the lateral and heading errors of the pose of the vehicle with respect to the reference path. Stemming from this, two different scenarios stand out: in order to adapt the bicycle model to the flow of data of the PP controller, two models for PP control that take as input the steering angle and give as output the LHE are derived in Sec.2.4, based on geometric rules for both straight and circular paths.

Eventually, a model of the DC servomotor is presented in Sec.2.5 to take into account the delay and dynamics introduced by the steering actuation mechanism.

2.1 Ackerman steering geometry

The fundamental basis for kinematic vehicle models is the Ackerman steering geometry assumption which assumes that the normal lines to the centre of each tire-plane must intersect at a common turning centre (see Fig.2.1).

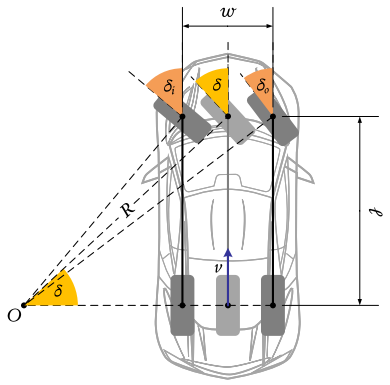

Figure 2.1: Ackerman steering geometry

Considering a front-wheel steering vehicle that is turning very slowly, there is a kinematic relation between the inner and the outer wheels that allows them to turn slip-free. With reference to Fig.2.1, the inner and the outer steering angles can be calculated as follows:

$$\begin{aligned} \tan\delta_i &= \frac{\ell}{R - \frac{w}{2}} \\ \tan\delta_o &= \frac{\ell}{R + \frac{w}{2}} \end{aligned} \tag{2.1}$$

Eliminating R:

$$R = \frac{1}{2}w + \frac{\ell}{\tan\delta_i} = -\frac{1}{2}w + \frac{\ell}{\tan\delta_o}$$

provides the Ackerman condition (2.2), which is expressed by the equation [9]:

$$\cot\delta_o - \cot\delta_i = \frac{w}{\ell} \tag{2.2}$$

The Ackerman condition can be used when the speed of the vehicle is small: lateral and centrifugal forces are negligible and the side-slip angle is considered to be zero. Under these assumptions, the four-wheel vehicle can be approximated by a two-wheel model whose steering angle δ is given by the cot-average of the inner and the outer angles:

$$\cot\delta = \frac{\cot\delta_o + \cot\delta_i}{2} = \frac{R}{\ell} \tag{2.3}$$

2.2 Global bicycle model

The bycicle model is a kinematic vehicle model characterized by the fact that the front and rear wheels of the car-like vehicle are constrained to move on a plane and lumped together respectively, with ℓ being the wheelbase distance. Only the front wheel is free to move around an axis normal to the plane of motion, to model steering. Under the assumption that the wheels are pure rolling without any side slip, the Pfaffian non-holonomic constraint for each wheel can be expressed as:

$$\dot{x}\sin\psi - \dot{y}\cos\psi = 0. \tag{2.4}$$

with x, y and ψ representing the pose of the wheel. It follows that the nonlinear equations which describe a driftless, rear wheel driving bicycle model [6], represented in Fig.2.2a, are:

$$\begin{aligned} \dot{x} &= \frac{\mathrm{d}x}{\mathrm{d}t} = v\cos\psi \\ \dot{y} &= \frac{\mathrm{d}y}{\mathrm{d}t} = v\sin\psi \\ \dot{\psi} &= \frac{\mathrm{d}\psi}{\mathrm{d}t} = \frac{v}{\ell}\tan\delta \end{aligned} \tag{2.5}$$

where the relation $\dot{\psi} = v/R$ between the yaw rate and the velocity of the car was exploited.

The state of the vehicle is represented by the vector $\left[x, y, \psi\right]^\top$, where x, y describe the position of the rear axis with respect to a global reference frame and ψ is the heading angle of the vehicle. A major drawback of this model is that it permits instantaneous steering angle change which can be problematic if the motion planning module generates solutions with such instantaneous changes [15]. This kinematic model is solely based on the Ackerman steering geometry of the vehicle, derived regardless of forces, torques and inertial effects in general and for this reason it is of practical use, widely employed in the literature due to its simplicity and sufficient performance at low speeds. When the vehicle is moving at higher speeds, the dynamic effects of some components become more prominent and need to be modelled appropriately. Anyway it is worth mentioning that Kong et al. in [10] proved the effectiveness of a kinematic bicycle model compared to a dynamic one in a prediction framework: they showed how, unexpectedly, the forecast error statistics are comparable for both models, especially when the kinematic model is sampled at a slower rate. So to sum up, on the one hand this model suffers from these flaws but, on the other hand, due to its remarkable simplicity, it allows to derive very efficient control laws for tracking a given path.

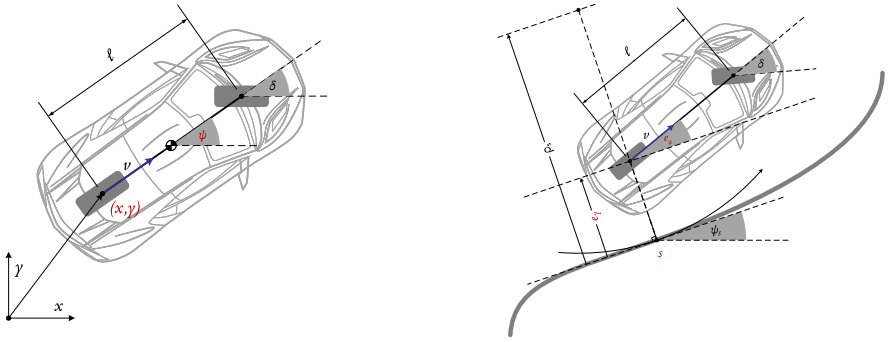

(a) Global **(b)** Local

Figure 2.2: Bicycle model

2.3 Local bicycle model

In the path tracking scenario in general it's useful to consider the relative pose with respect to a given path. With this in mind, a spatial-based error model in path coordinates can be derived from the global one (2.5), through a change of coordinates [6, 8]:

$$\begin{aligned} \dot{s} &= \frac{\rho_s(s) v \cos e_\psi}{\rho_s(s) - e_y} \\ \dot{e}_y &= v \sin e_\psi \\ \dot{e}_\psi &= \frac{v}{\ell} \tan\delta - \dot{\psi}_s(s) = \frac{v}{\ell} \tan\delta - \frac{v \cos e_\psi}{\rho_s(s) - e_y} \end{aligned} \tag{2.6}$$

Local quantities are described in Fig.2.2b: s is the projected vehicle position along the lane center line, ρ_s is the radius of curvature of the road and ψ_s is the road heading angle. Stemming from

this model, two cases will be of particular interest in the following treatise. The case of straight path can be obtained by setting the road heading rate ψ_s to 0, or equivalently by taking the limit $\rho_s \to \infty$:

$$\begin{aligned} \dot{s} &= v \cos e_\psi \\ \dot{e}_y &= v \sin e_\psi \\ \dot{e}_\psi &= \frac{v}{\ell} \tan \delta \end{aligned} \tag{2.7}$$

In this particular case, the local and the global model coincide by taking the path as the x-axis of the world frame so that (s, e_y, e_ψ) become the coordinates (x, y, ψ) of the vehicle [6]. The other particular case is that of circular path, where the radius of curvature of the road ρ_s is considered to be constant and different from 0:

$$\begin{aligned} \dot{s} &= \frac{\rho_s v \cos e_\psi}{\rho_s - e_y} \\ \dot{e}_y &= v \sin e_\psi \\ \dot{e}_\psi &= \frac{v}{\ell} \tan \delta - \dot{\psi}_s = \frac{v}{\ell} \tan \delta - \frac{v \cos e_\psi}{\rho_s - e_y} \end{aligned} \tag{2.8}$$

This kind of error models differ from the global one for the fact of relying only on local quantities, without any dependence on the global pose of the car.

2.4 Model for PP control

The nonlinear local model (2.6) can be recast from a control viewpoint, assuming the steering angle δ as input $\mathbf{u}$ and, in view of a PP type of control, the LHE α as output $\mathbf{y}$:

$$\begin{aligned} \dot{\mathbf{x}} = \mathbf{f}_x(\mathbf{x}, \mathbf{u}) &:= \begin{bmatrix} v \sin e_\psi \\ \dfrac{v}{\ell} \tan \delta - \dot{\psi}_s(s) \end{bmatrix} \\ \mathbf{y} = \mathbf{f}_y(\mathbf{x}) &:= \arcsin \frac{e_d(\mathbf{x})}{L_d} \end{aligned} \tag{2.9}$$

where the trigonometric relation between the LHE and the LLE:

$$e_d = L_d \sin \alpha \tag{2.10}$$

was used for the output function.
For sake of convenience, hereinafter the error state vector will be referred to as $\mathbf{x} = \left[e_y, e_\psi\right]^\top$. In general, the lack of a closed form characterization of the output function prevents a thorough study of the closed loop control system. If a reliable Global Positioning System was available, (2.11) could be expressed by:

$$\alpha = \arctan \frac{y_{L_d} - y}{x_{L_d} - x} - \psi \tag{2.11}$$

where ψ is the yaw angle of the vehicle and x_{L_d}, y_{L_d} are the coordinate of the lookahead point with the greatest value of s to uniquely define a control [15]. In this scenario it would be possible

to to define a nonlinear state feedback control law, anyway in a real scenario, like in the BFMC one, global coordinates are usually not reliable if not available at all (e.g. in a tunnel).
As opposed to this, in the two local scenarios mentioned above, it is possible to derive a closed form relation between the LLE and the state by resorting to simple geometric rules [14].

2.4.1 *Circular scenario*

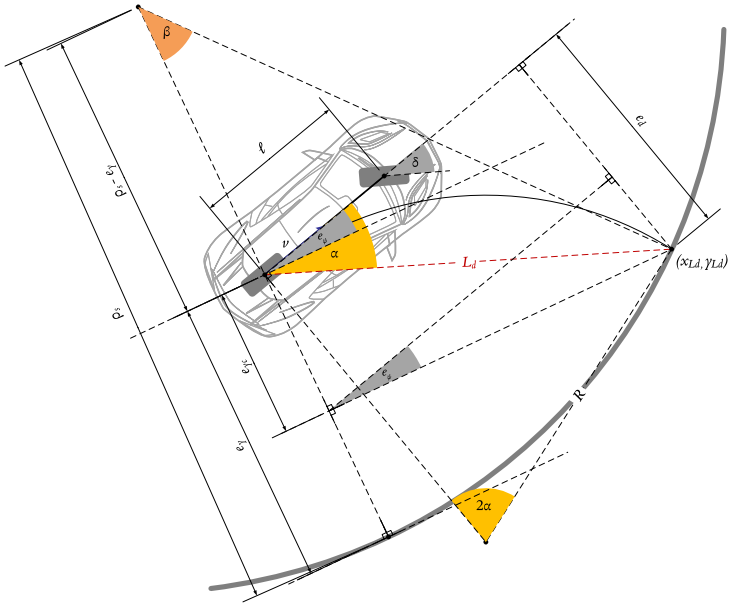

Figure 2.3: Pure Pursuit geometry in the circular scenario

In the case of circular path, represented in Fig.2.3, by resorting to the law of cosines and other trigonometric identities, the following relations hold true:

$$L_d^2 = {\rho_s}^2 + (\rho_s - e_y)^2 - 2\rho_s(\rho_s - e_y)\cos\beta$$
$$\cos\beta = -\frac{L_d^2 - {\rho_s}^2 - (\rho_s - e_y)^2}{2\rho_s(\rho_s - e_y)}$$

The *circular lateral error* e_{y_c} is then defined as:

$$e_{y_c} = \rho_s\cos\beta - (\rho_s - e_y) = \frac{-L_d^2 - e_y^2 + 2\rho_s e_y}{2(\rho_s - e_y)} \tag{2.12}$$

With reference to Fig.2.3, the LLE in the circular path case is expressed by the nonlinear relation:

$$e_d = e_{y_c}\cos e_\psi + \sqrt{L_d^2 - e_{y_c}}\sin e_\psi \tag{2.13}$$

Under the local assumption that $|e_d| < L_d$, the resulting system, obtained be putting together the model (2.9) with the LLE (2.13), is:

$$\begin{aligned}\dot{\mathbf{x}} &= \begin{bmatrix} v \sin e_\psi \\ \frac{v}{\ell} \tan\delta - \frac{v \cos e_\psi}{\rho_s - e_y} \end{bmatrix} \\ \mathbf{y} &= \arcsin \frac{\frac{-L_d^2 - e_y^2 + 2\rho_s e_y}{2(\rho_s - e_y)} \cos e_\psi + \sqrt{L_d^2 - \left(\frac{-L_d^2 - e_y^2 + 2\rho_s e_y}{2(\rho_s - e_y)}\right)^2} \sin e_\psi}{L_d}\end{aligned} \tag{2.14}$$

The origin $\mathbf{x}_0 = [0, 0]^\top$, the input $\mathbf{u}_0 = \arctan \frac{\ell}{\rho_s}$ and the output $\mathbf{y}_0 = \arcsin -\frac{L_d}{2\rho_s}$ are an equilibrium configuration for the system (2.14) which can be linearized as (see App.A):

$$\Sigma_c : \begin{cases} \dot{\tilde{\mathbf{x}}} = \nabla_x \mathbf{f}_x(\mathbf{x}_0)(\mathbf{x} - \mathbf{x}_0) + \nabla_u \mathbf{f}_x(\mathbf{u}_0)(\mathbf{u} - \mathbf{u}_0) := A_c \tilde{\mathbf{x}} + B_c \tilde{\mathbf{u}} \\ \tilde{\mathbf{y}} = \nabla_x \mathbf{f}_y(\mathbf{x}_0)(\mathbf{x} - \mathbf{x}_0) := C_c \tilde{\mathbf{x}} \end{cases} \tag{2.15}$$

where $\tilde{\mathbf{x}} = \mathbf{x} - \mathbf{x}_0$, $\tilde{\mathbf{u}} = \mathbf{u} - \mathbf{u}_0$, $\tilde{\mathbf{y}} = \mathbf{y} - \mathbf{y}_0$ and:

$$\begin{aligned} A_c &= \left[\begin{matrix} 0 & v \cos e_\psi \\ -\frac{v \cos e_\psi}{(\rho_s - e_y)^2} & \frac{v}{\rho_s - e_y} \sin e_\psi \end{matrix} \right]\Bigg|_{\mathbf{x}_0} = \begin{bmatrix} 0 & v \\ -\frac{v}{{\rho_s}^2} & 0 \end{bmatrix} \\ B_c &= \left[\begin{matrix} 0 \\ \frac{v}{\ell} \frac{1}{\cos^2 \delta} \end{matrix} \right]\Bigg|_{\mathbf{u}_0} = \begin{bmatrix} 0 \\ \frac{v}{\ell} \gamma \end{bmatrix} \\ C_c &= \left[\begin{matrix} \frac{1}{\sqrt{1 - \left(\frac{e_d}{L_d}\right)^2}} \frac{1}{L_d} \frac{\partial e_d}{\partial e_y} & \frac{1}{\sqrt{1 - \left(\frac{e_d}{\ell}\right)^2}} \frac{1}{L_d} \frac{\partial e_d}{\partial e_\psi} \end{matrix} \right]\Bigg|_{\mathbf{x}_0} = \begin{bmatrix} \lambda & 1 \end{bmatrix} \end{aligned}$$

with $\gamma = \frac{1}{\cos^2\left(\arctan \frac{\ell}{\rho_s}\right)}$ and $\lambda = \frac{2{\rho_s}^2 - L_d^2}{L_d \rho_s \sqrt{4{\rho_s}^2 - L_d^2}}$.
The corresponding transfer function from the linearized steering angle to the linearized LHE can be computed using standard systems theory rules:

$$P_C(s) = C_c [sI - A_c]^{-1} B_c = \frac{v^2 \lambda \gamma}{\ell} \frac{1 + s\frac{1}{v\lambda}}{s^2 + \frac{v^2}{{\rho_s}^2}} \tag{2.16}$$

2.4.2 *Straight scenario*

The case of straight path, which is represented in Fig.2.4, can be derived either by resorting to geometric rules like in the circular case, or it can be seen as a limit case by taking the limit:

$$\lim_{\rho_s \to \infty} e_{y_c} = e_y$$

According to this, the LLE keeps the same form as in the circular case:

$$e_d = e_y \cos e_\psi + \sqrt{L_d^2 - e_y^2} \sin e_\psi \tag{2.17}$$

The resulting system obtained embedding the LLE (2.17) inside the model (2.9) is:

$$\begin{aligned} \dot{\mathbf{x}} &= \begin{bmatrix} v \sin e_\psi \\ \dfrac{v}{\ell} \tan \delta \end{bmatrix} \\ \mathbf{y} &= \arcsin \frac{e_y \cos e_\psi + \sqrt{L_d^2 - e_y^2} \sin e_\psi}{L_d} \end{aligned} \tag{2.18}$$

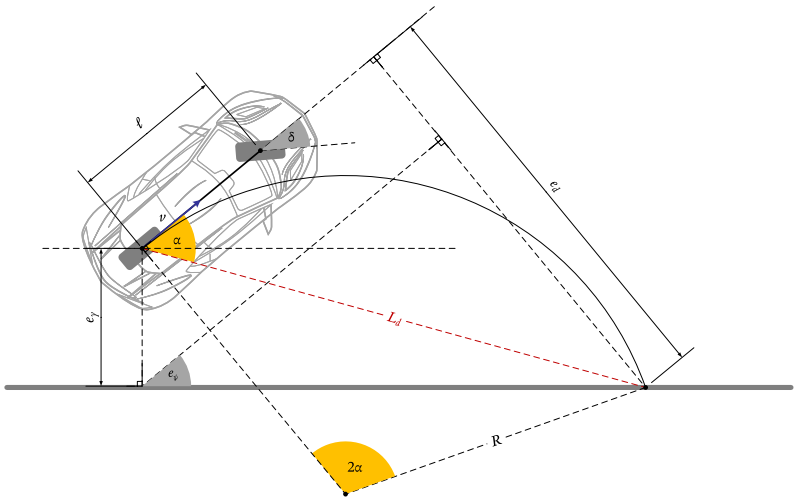

Figure 2.4: Pure Pursuit geometry in the straight scenario

In this case the origin of the state space $\mathbf{x}_0 = [0, 0]^\top$ is an equilibrium configuration with both null input $\mathbf{u}_0 = 0$ and output $\mathbf{y}_0 = 0$ and the linearized model can be derived as a limit case of the circular one, too (see App.A):

$$\Sigma_s : \begin{cases} \dot{\tilde{\mathbf{x}}} = \nabla_x \mathbf{f}_x(\mathbf{x}_0)(\mathbf{x} - \mathbf{x}_0) + \nabla_u \mathbf{f}_x(\mathbf{u}_0)(\mathbf{u} - \mathbf{u}_0) := A_s \tilde{\mathbf{x}} + B_s \tilde{\mathbf{u}} \\ \tilde{\mathbf{y}} = \nabla_x \mathbf{f}_y(\mathbf{x}_0)(\mathbf{x} - \mathbf{x}_0) := C_s \tilde{\mathbf{x}} \end{cases}$$

where

$$A_s = \left[\begin{matrix} 0 & v \cos e_\psi \\ 0 & 0 \end{matrix} \right]\Bigg|_{\mathbf{x}_0} = \begin{bmatrix} 0 & v \\ 0 & 0 \end{bmatrix}$$

$$B_s = \left[\begin{matrix} 0 \\ \frac{v}{\ell} \frac{1}{\cos^2 \delta} \end{matrix} \right]\Bigg|_{\mathbf{u}_0} = \begin{bmatrix} 0 \\ \frac{v}{\ell} \end{bmatrix}$$

$$C_s = \left[\frac{1}{\sqrt{1-\left(\frac{e_d}{L_d}\right)^2}} \frac{1}{L_d} \frac{\partial e_d}{\partial e_y} \quad \frac{1}{\sqrt{1-\left(\frac{e_d}{\ell}\right)^2}} \frac{1}{L_d} \frac{\partial e_d}{\partial e_\psi} \right]\Bigg|_{\mathbf{x}_0} = \begin{bmatrix} \frac{1}{L_d} & 1 \end{bmatrix}$$

The transfer function associated to the linearized model in the straight case is:

$$P_S(s) = C_s[sI - A_s]^{-1}B_s = \frac{v^2}{\ell L_d} \frac{1 + s\frac{L_d}{v}}{s^2} \tag{2.19}$$

2.5 STEERING SYSTEM MODEL

Both the global (2.5) and the local (2.6) models suffer from the fact that the input steering signal acts immediately on the system, unlike what happens in the real car. In practice the steering action is performed by a DC servomotor controlled by a PWM signal with variable duty cycle. It can be verified that there is some delay between when the signal is applied and when the steering wheel actually sets to the reference steering angle. The delay in between when the reference is applied and when the wheel starts turning is called *static delay* τ_d and can be due to the mechanical actuation mechanism, the electronics that controls it or the software architecture. Once the wheel starts turning, it shows a certain dynamics in the movement which can be modelled through a first order system with time constant τ, hereinafter referred to as *steering lag*. The overall steering dynamics can thus be modelled by the differential equation [27]:

$$\tau\dot{\delta}(t) = -\delta(t - \tau_d) + \delta_r(t) \tag{2.20}$$

By applying the Laplace transform on both sides of (2.20), the FOPTD transfer function from the steering angle reference to the actual steering angle is obtained:

$$D(s) = \frac{e^{-\tau_d s}}{1 + \tau s} \tag{2.21}$$

CHAPTER

3 Pure Pursuit control

The PP controller is a proportional geometric controller on an angle, called the *Lookahead Heading Error*, defined on a point on the reference path ahead of the vehicle by a distance L_d, called the *lookahead distance*. Due to its simplicity of implementation and performance at low speeds, it represents a valid candidate for lateral control of the 1:10 scale vehicle in the BFMC scenario.

The basic PP controller is widely discussed is in Sec.3.1 with particular attention to its only tunable parameter, namely the lookahead distance, in terms of tracking accuracy and robustness.

In our scenario, the LHE is computed by means of a Convolutional Neural Network and is assumed to be available at a fixed lookahead distance, therefore new control strategies need to be adopted in order to cope with this constraint.

In this Chapter, three contributions to the basic PP control law based on the only data available from the CNN will be proposed and analyzed, both in the straight and circular scenarios. The first strategy consists of a proportional gain and yields to the *Proportional Pure Pursuit* (PP-P) controller which is analyzed in Sec.3.2.

The availability of a noiseless estimation from the CNN allows to augment the PP-P control law with an added derivative term on the LHE so, in Sec.3.3, the *Proportional Derivative Pure Pursuit* (PP-PD) control law is discussed.

Eventually, in Sec.3.4, a *PP-based velocity reference generation* technique is presented with the aim of driving the vehicle at a desired maximum speed, avoiding excessive lateral accelerations on corners.

3.1 The Basic Pure Pursuit (PP) controller

The PP controller lies in the subset of geometric controllers, i.e. controllers that rely on the geometry of a kinematic model of the vehicle, regardless of dynamic effects. In this section a detailed geometric derivation of the PP control law and its tuning strategy is presented, along with its main drawbacks in the current framework. In view of a time-delay stability analysis, a linearized version of the controller is derived, too.

3.1.1 *Pure Pursuit geometry*

The Pure Pursuit controller is a PTC based on fitting an arc of circumference through the vehicle's current configuration to a point on the reference path ahead of the vehicle by a distance L_d. The arc is defined as passing through the rear axis of the car and the point on the path ahead by one lookahead distance with the arc tangent to the car's heading.

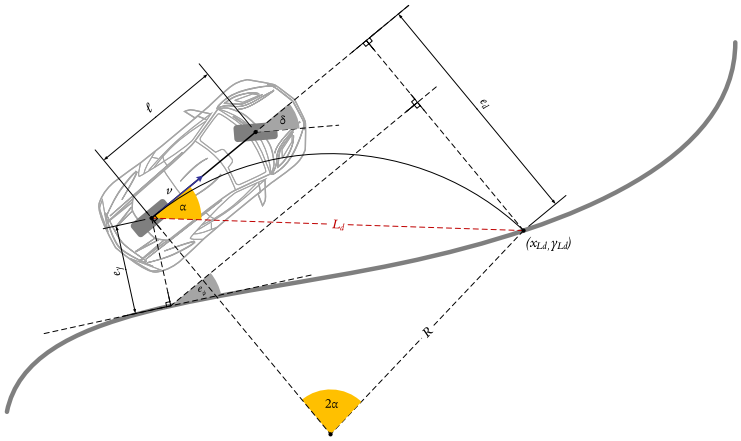

Figure 3.1: Pure Pursuit controller

With reference to Fig.3.1, by resorting to the rule of sines and other basic geometric rules, the radius of the fitted arc can be derived as:

$$\begin{aligned} \frac{L_d}{\sin(2\alpha)} &= \frac{R}{\sin\left(\frac{\pi}{2} - \alpha\right)} \\ \frac{L_d}{2\sin\alpha\cos\alpha} &= \frac{R}{\cos\alpha} \\ R = \frac{1}{\kappa} &= \frac{L_d}{2\sin\alpha} \end{aligned} \tag{3.1}$$

where κ is the curvature of the interpolated arc of circumference.
The Ackerman steering geometry for a kinematic single-track bicycle model gives the relation:

$$\tan\delta = \frac{\ell}{R} = \ell\,\kappa \tag{3.2}$$

Therefore, given the LHE α as input, the PP steering angle control law can be derived:

$$\delta = \arctan\frac{2\ell\sin\alpha}{L_d} = \arctan(\ell\kappa) \tag{3.3}$$

Beyond geometric motivation, it is interesting to investigate equilibria and stability of the nonlinear closed loop control system in both the scenarios introduced above. In App.B asymptotic stability for the origin of the state space is proved in both the straight and the circular cases by linearization. Moreover a Lyapunov approach is also presented: based on [17], stability is proved in the the straight scenario by resorting to a suitable Lyapunov function, while in the circular scenario a way of constructing such Lyapunov function is introduced based on state trajectories of the closed loop system.

3.1.2 *The lookahead distance*

A better understanding of this controller can be gained by recasting previous quantities as a function of the LLE, exploiting the relation (2.10). The curvature of the fitted arc is directly proportional to the LLE by the proportionality gain $2/L_d^2$:

$$\kappa = \frac{2\sin\alpha}{L_d} = \frac{2}{L_d^2} e_d \quad \Rightarrow \quad \kappa \propto e_d \tag{3.4}$$

Therefore the PP controller can be seen as a nonlinear proportional controller on the lookahead cross-track error e_d:

$$\delta = \arctan \frac{2\ell e_d}{L_d^2} \tag{3.5}$$

As the LLE increases, so does the curvature of the fitted arc and the vehicle is driven towards the path more aggressively. This behaviour is regulated by the gain $2/L_d^2$, which is inversely proportional to the lookahead distance squared.
As this analysis may suggest, the main shortcoming of the PP controller is the selection of the lookahead distance L_d. Indeed, as usual in path tracking control, a trade-off must be performed between stability and tracking performance. It is useful to point out how the action of this controller behaves like a human driver with shorter lookahead distances that results in more accuracy in following the path but may lead to oscillatory behaviours and, on the other hand, too large lookahead distances which provides smoother tracking but will result in the "cutting-corners" effect while approaching tight curves [21]. In fact, the geometry underlying this controller ignores the curvature of the path ahead, approximating it to be constant.
The main approach to solve this trade-off is choosing the lookahead distance proportional to the velocity of the vehicle. A common way of implementing this method is to scale the lookahead distance with the longitudinal velocity by a constant k that can be tuned on a variety of courses and speeds to find a value that can perform well over the operating space of the vehicle [21, 22]:

$$\delta = \arctan \frac{2\ell \sin\alpha}{kv} \tag{3.6}$$

However it is difficult to converge to the path smoothly when there is a large cross track error due to the fact that the PP strategy does not take into account the alignment of the direction of the path and the heading of the vehicle at the same time. In alternative to this, in [1] an innovative approach that assigns an offset distance to the look-ahead point according to geometric rules is presented.

3.1.3 *Controller linearization*

Using the first order Taylor approximation of the arctan and the sin functions, the basic PP controller can be linearized as:

$$\delta = \arctan \frac{2\ell \sin\alpha}{L_d} \approx \frac{2\ell}{L_d}\alpha \tag{3.7}$$

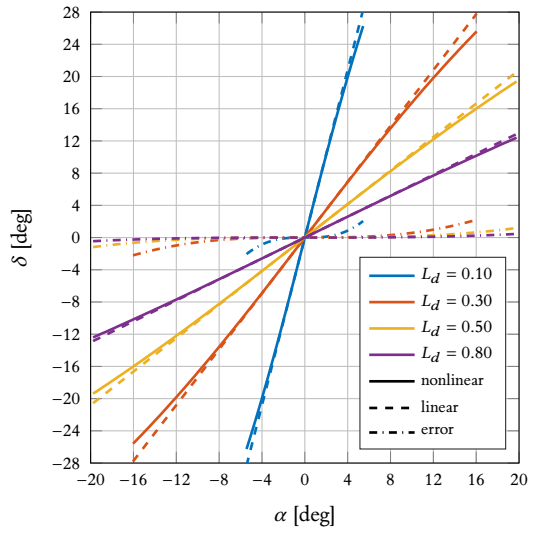

Figure 3.2: Error introduced by the linearization of the PP control law for $\delta \in [-28, 28]$ deg

In Fig.3.2 the two functions are plotted for δ in between the saturation bounds imposed by the steering mechanism.
This linearized form of the controller gives some more insights into the behaviour of the PP strategy, from a control viewpoint. As discussed in [16], under straight line assumption (see Fig.2.4) and small LHE, $\alpha \approx \sin\alpha \approx e_\psi + (\alpha - e_\psi) \approx \dot{e}_y/v + e_y/L_d$. This approximation allows to recast the proportional form (3.7) on the future measure α into a proportional derivative controller on the current lateral error e_y,:

$$\delta \approx \frac{2\ell}{vL_d}\left(\dot{e}_y + \frac{v}{L_d}e_y\right) \qquad \xrightarrow{\mathscr{L}} \qquad \frac{2\ell}{L_d^2}\left(1 + s\frac{L_d}{v}\right)E_y(s)$$

Therefore the basic PP controller, for a small neighbourhood of the origin of the state space, has the effect of introducing a stable zero and a proportional gain with the lookahead distance having a twofold coupled effect in tuning the trade-off between these two contributions. The first is inversely proportional to the lookahead distance squared and regulates the aggressiveness of the control action; the second depends on the ratio between the lookahead distance and the velocity and regulates the anticipative action thus enabling phase recovery around the natural frequency of the system [16].
Anyway, as already mentioned above, in our scenario L_d is fixed so here follow three possible strategies to to tune these two behaviours with an insight from classical control theory.

3.2 The Proportional Pure Pursuit (PP-P) controller

In order to tune the aggressiveness of the PP controller in a constant lookahead distance scenario, a proportional gain can be added in front of the basic PP control law (3.3). The proposed PP-P

control law is:

$$\delta = K_{pp}^P \arctan \frac{2\ell \sin \alpha}{L_d} = K_{pp}^P \arctan \frac{2\ell e_d}{L_d^2} \approx K_{pp}^P \frac{2\ell}{L_d} \alpha \tag{3.8}$$

The proportional gain intuitively plays the opposite role to the lookahead distance in regulating the aggressiveness of the controller, with higher gains leading to a more responsive system and lower gains improving robustness at higher velocities.
Anyway, it must be noticed that a lower bound for this gain with respect to the combination (v, L_d) is expected both in the straight and in the circular scenarios due to the fact that small gains could result in a slow steering action that may drive the car out of lane.
In addition to this, in the circular scenario the lower bound is expected to increase in relation to the path curvature since a minimum steering angle is necessary to make the curve; in this case also an upper bound is expected in order to avoid the vehicle to cut the curve.

3.2.1 *Straight scenario*

Applying the PP-P control law (3.8) to the straight path model (2.7) gives the closed loop system:

$$\begin{aligned} \dot{e}_y &= v \sin e_\psi \\ \dot{e}_\psi &= \frac{v}{\ell} \tan \left(-K_{pp}^P \arctan \frac{2\ell e_d}{L_d^2} \right) \end{aligned} \tag{3.9}$$

In this case the curvature of the path is zero and the equilibrium configurations for the lateral error can be obtained by imposing zero heading error into the second differential equation, thus obtaining the condition:

$$K_{pp}^P \arctan \frac{2\ell e_y}{L_d^2} = 0 \quad \Rightarrow \quad e_y = 0$$

This implies that, in the straight path case, the perfect tracking condition is not affected by the proportional gain that here allows to tune the performance of the controller for a fixed lookahead distance. Murphy in [13] already analyzed this case, in a linearized scenario, with respect to the root locus of the delay free system. Applying the linearized PP-P controller to the transfer function (2.19), yields the following closed loop characteristic polynomial:

$$\Delta(s) := d(s) + K_{pp}^P n(s) = s^2 + K_{pp}^P \frac{2v^2}{L_d^2} \left(1 + s \frac{L_d}{v} \right) \tag{3.10}$$

The shape of the root locus of this closed loop system is represented in Fig.3.3
In Fig.3.4 it is plotted the response of the closed loop system varying K_{pp}^P for $L_d = 0.5\,\mathrm{m}$ in the delay-free case and it can be noticed how steady-state zero tracking error is reached, with different dynamics, in every case. All in all, this control action is still not enough to cope with the missing DoF on the anticipative action introduced by the basic PP.

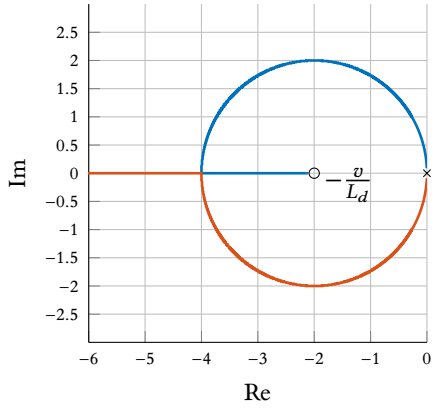

Figure 3.3: Root locus of the linearized closed loop system applying the PP-P controller to the straight scenario with $L_d = 0.5\,\mathrm{m}$ and $v = 1,\mathrm{m\,s^{-1}}$.

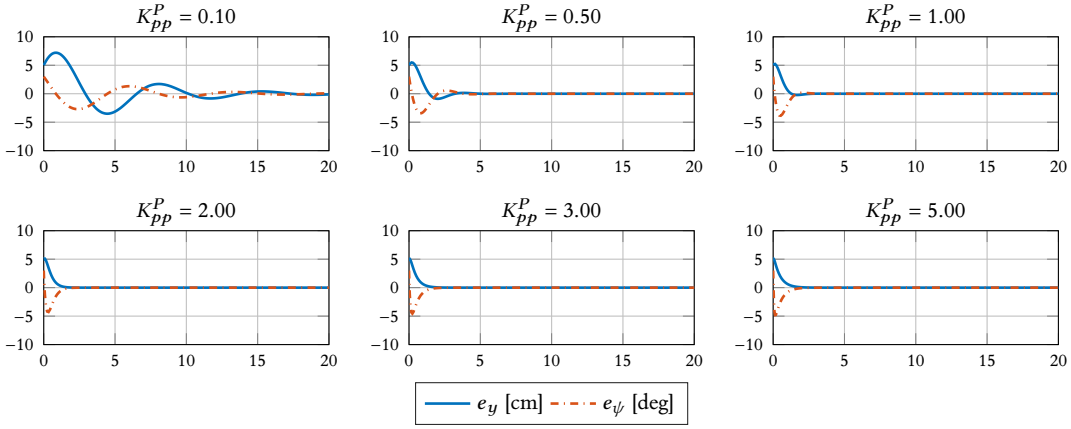

Figure 3.4: Simulation of PP-P straight path tracking with initial condition $\mathbf{x}_0 = [0.05, 3\pi/180]$, varying K_{pp}^P for fixed $L_d = 0.5\,\mathrm{m}$, in the delay-free case.

3.2.2 *Circular scenario*

Applying the PP-P control law (3.8) to the circular path model (2.8), the following state feedback closed loop system is obtained:

$$\begin{aligned}\dot{e}_y &= v \sin e_\psi \\ \dot{e}_\psi &= \frac{v}{\ell} \tan\left(-K_{pp}^P \arctan \frac{2\ell e_d}{L_d^2}\right) - \frac{v\cos e_\psi}{\rho_s - e_y}\end{aligned} \tag{3.11}$$

The first equation entails null heading error $e_\psi = 0$ at the equilibrium. Imposing this constraint into the second equation, leads to the following condition for lateral error equilibrium points:

$$\tan\left(-K_{pp}^P \arctan\frac{2\ell e_{y_c}}{L_d^2}\right) = \frac{\ell}{\rho_s - e_y}$$

Rearranging this equation yields a nonlinear relation between lateral error equilibrium points and their respective gains:

$$K_{pp}^P = -\frac{\arctan\frac{\ell}{\rho_s - e_y}}{\arctan\frac{2\ell e_{y_c}}{L_d^2}} \tag{3.12}$$

Function (3.12) is plotted in Fig.3.5 for three different values of fixed lookahead distance and $K_{pp}^P > 0$. It can be verified that (3.12) has a vertical asymptote for $e_{y_c} = 0$:

$$-e_y^2 + 2\rho_s e_y - L_d^2 = 0 \quad \Rightarrow \quad e_y = \rho_s - \sqrt{{\rho_s}^2 - L_d^2}$$

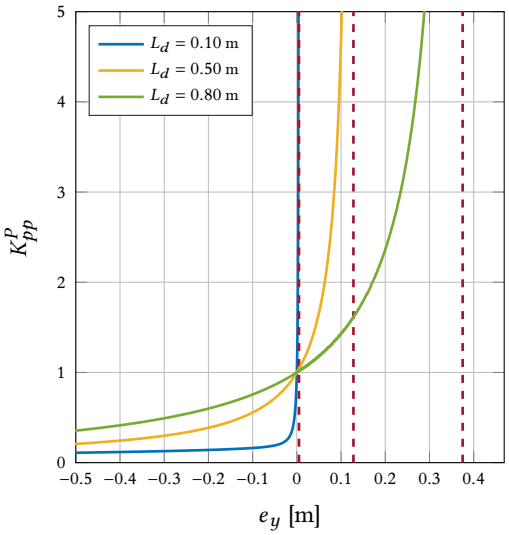

Figure 3.5: Equlibrium configurations (e_y, K_{pp}^P) of the closed loop system (3.11) for $e_\psi = 0$, $v = 0.3\,\mathrm{m\,s^{-1}}$ and $\rho_s = 1.04\,\mathrm{m}$.

Regardless of the lookahead distance, the function crosses the ordinate axis only for $K_{pp}^P = 1$ which means that the basic pure pursuit controller is the only configuration that guarantees perfect tracking of a circular path. If $K_{pp}^P > 1$, then the lateral error equilibrium point increases and a bias is introduced up to the asymptote that ideally corresponds to the vehicle being inside the circle with zero heading error and pointing towards the lookahead point. Therefore it can be depicted that the curvature of the path sets a limit to the inner bias introduced by increasing the proportional gain.

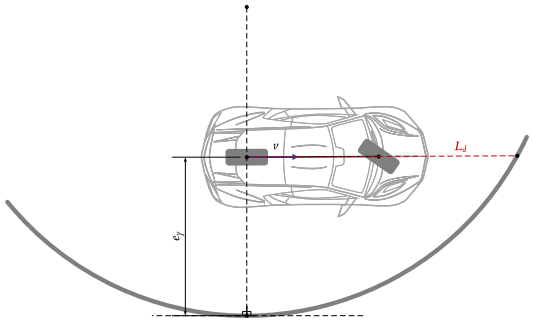

Figure 3.6: Limit equilibrium configuration for the PP-P controller in the circular scenario

If $K_{pp}^P < 1$, then the lateral error equilibrium point decreases up to $-\infty$: this is the case where the vehicle is tracking a circle which is wider than the reference one.
Eventually it can be noticed that the lookahead distance tunes an other trade-off between the lateral error bias and the sensitivity to gain variations at the equilibrium configuration: in particular, the longer the lookahead distance, the lower the sensitivity to gain variations around the perfect tracking condition with $K_{pp}^P = 1$; the smaller the lookahead distance, the smaller the upper bound to the bias introduced by varying the gain. Therefore, in the circular case upper and lower bounds for K_{pp}^P coincide and are equal to 1. In view of reducing the effect due to nonidealities that may vary the gain it is desirable to fix $L_d < \rho_s$ big enough.
In Fig.3.7 various responses of the delay free system (2.9) in the circular case are plotted varying the proportional gain for fixed $L_d = 0.5$ m. It can be noticed how perfect heading tracking is achieved in all the configurations. On the other hand the lateral error settles at different values as the gain varies.

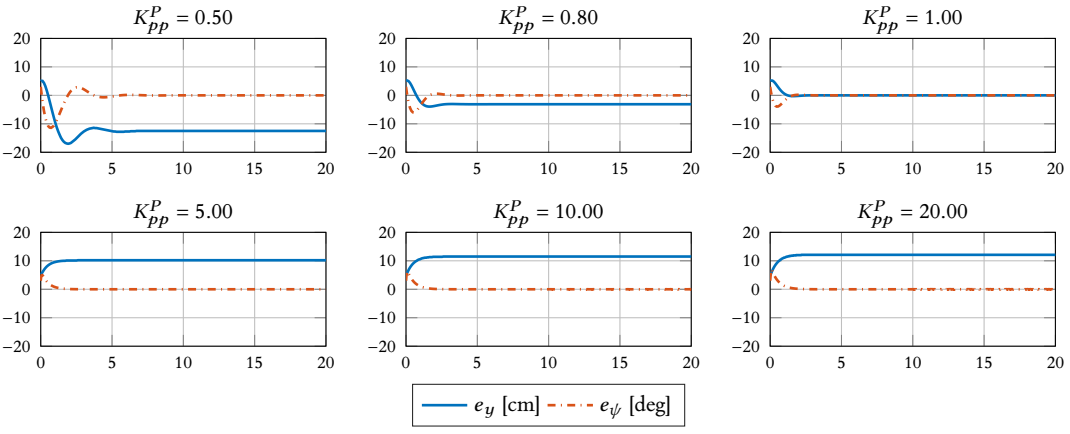

Figure 3.7: Simulation of PP circular path tracking with $\rho_s = 1.04$ m, initial condition $\mathbf{x}_0 = [0.05, 3\pi/180]$, varying K_{pp}^P for fixed $L_d = 0.5$ m in the delay-free case. It can be noticed that, if $K_{pp}^P < 1$, the steady state lateral error settles to a negative value, while if $K_{pp}^P > 1$, the error becomes positive and tends to the limit value of 0.1281 m.

3.3 The Proportional Derivative Pure Pursuit (PP-PD) controller

The analysis in the previous Section proved how the proportional gain can be used only as an additional DoF to tune the aggressiveness of the system in the straight scenario, having no effect in tuning the anticipatory action which depends solely on the relation between the velocity and the lookahead distance. Indeed in Sec.3.1.3 the anticipative action of the basic PP control law was proved to be modeled by a stable zero in $-v/L_d$, when expressed with respect to the lateral error e_y in a linearized scenario.
In order to recover such missing DoF, the availability of a noise-free estimation from the CNN can be successfully used to introduce a derivative contribution on the LHE.
The proposed PP-PD control law is:

$$\delta_r = K_{pp}^P \arctan \frac{2\ell \sin\alpha}{L_d} + K_{pp}^D \frac{\mathrm{d}\alpha}{\mathrm{d}t} \tag{3.13}$$

As previously done, an insight on the new control action can be gained by linearization:

$$\delta_r \approx K_{pp}^P \frac{2\ell}{L_d}\alpha + K_{pp}^D \frac{\mathrm{d}\alpha}{\mathrm{d}t} \quad \xrightarrow[\mathscr{L}]{} \quad K_{pp}^P \frac{2\ell}{L_d}\left(1 + s\frac{K_{pp}^D}{K_{pp}^P}\frac{L_d}{2\ell}\right)A(s) \tag{3.14}$$

Recasting (3.14) as a function of the lateral error in the straight case gives the proportional derivative control law:

$$\delta \approx \frac{K_{pp}^D}{v}\ddot{e}_y + \left(\frac{2\ell}{vL_d}K_{pp}^P + \frac{K_{pp}^D}{L_d}\right)\dot{e}_y + \frac{2\ell}{L_d^2}K_{pp}^P e_y \quad \xrightarrow[\mathscr{L}]{} \quad K_{pp}^P \frac{2\ell}{L_d^2}\left(1 + s\frac{L_d}{v}\right)\left(1 + s\frac{L_d}{2\ell}\frac{K_{pp}^D}{K_{pp}^P}\right) \tag{3.15}$$

Therefore the PP-PD controller has the effect of augmenting the PP-P controller by introducing an additional zero that depends on the ratio between the proportional and the derivative gains.

3.3.1 *Straight scenario*

Applying the linearized PP-PD controller to the transfer function (2.19), yields the following closed loop characteristic polynomial:

$$\Delta(s) := d(s) + K_{pp}^P n(s) = s^2 + K_{pp}^P \frac{2v^2}{L_d^2}\left(1 + s\frac{K_{pp}^D}{K_{pp}^P}\frac{L_d}{2\ell}\right)\left(1 + s\frac{L_d}{v}\right) \tag{3.16}$$

The additional real stable zero depends on the ratio between the proportional and the derivative gain, in particular if

$$\frac{K_{pp}^D}{K_{pp}^P}\frac{L_d}{2\ell} > \frac{v}{L_d} \quad \Longrightarrow \quad \frac{K_{pp}^D}{K_{pp}^P} > \frac{2L_d}{v} \tag{3.17}$$

then the additional zero is less than the zero introduced by the PP action in absolute value, thus introducing a slower dynamics than the PP-P case.

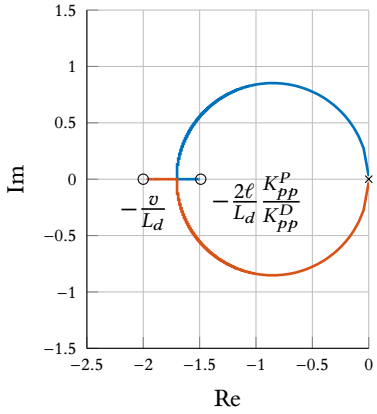

Figure 3.8: Root locus of the linearized closed loop system applying the PP-PD controller to the straight scenario with $L_d = 0.5\,\text{m}$, $v = 1\,\text{m}\,\text{s}^{-1}$ and $K_{pp}^D/K_{pp}^P = 0.7$.

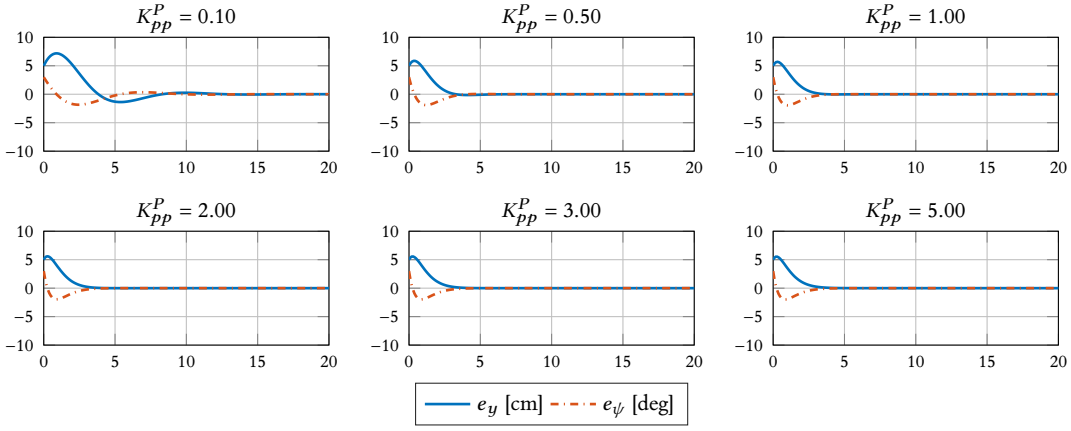

Figure 3.9: Simulation of PP-PD straight path tracking with initial condition $\mathbf{x}_0 = [0.05, 3\pi/180]$, varying K_{pp}^P for fixed $L_d = 0.5\,\text{m}$ and $K_{pp}^D/K_{pp}^P = 0.7$, in the delay-free case.

3.3.2 *Circular scenario*

Applying the PP-PD control law (3.8) with unitary K_{pp}^P to the circular path model (2.8), the following state feedback closed loop system is obtained:

$$\begin{aligned} \dot{e}_y &= v \sin e_\psi \\ \dot{e}_\psi &= \frac{v}{\ell} \tan\left(-\arctan \frac{2\ell e_d}{L_d^2} - K_{pp}^D \frac{\mathrm{d}\alpha}{\mathrm{d}t} \right) - \frac{v \cos e_\psi}{\rho_s - e_y} \end{aligned} \tag{3.18}$$

The origin remains an equilibrium point but the derivative gain has the effect of slowing the dynamics of the heading error, thus reducing the overshoot. A deeper insight on its effect on the dynamics of the closed loop response can be gained by observing how the roots of

the characteristic polynomial of the linearized closed loop system vary as a function of the derivative gain. Applying the linearized PP-PD controller to the transfer function (2.16), yields the following closed loop characteristic polynomial:

$$\begin{aligned}\Delta(s) := d(s) + n(s) &= \left(s^2 + \frac{v^2}{{\rho_s}^2}\right) + \frac{v^2\lambda\gamma}{\ell}\left(1 + s\frac{L_d}{v}\right)\left(\frac{2\ell}{L_d} + K_{pp}^D\, s\right) \\ &= \left(1 + \frac{v\lambda\gamma L_d}{\ell}K_{pp}^D\right)s^2 + \frac{v^2\lambda\gamma}{\ell}\left(\frac{2\ell}{v} + K_{pp}^D\right)s + \frac{v^2}{{\rho_s}^2} + \frac{2v^2\lambda\gamma}{L_d}\end{aligned} \tag{3.19}$$

It can be verified that for increasing K_{pp}^D, the roots of this polynomial tend to the imaginary axis from the left, thus leading to slower elementary modes. In this case it is not possible to control the aggressiveness of the system by changing the proportional gain, so the derivative gain alone, has the only effect of damping oscillations and therefore improves tracking accuracy. Simulations of the nonlinear control system are reported in Fig.3.10 for varying K_{pp}^D and unitary K_{pp}^P. It can be noticed how increasing the derivative gain slightly reduces the overshoot and slows down the response. Anyway, as the gain becomes too big, the derivative contribution gets bigger than the PP one and saturations on both the control and state variables occur: for increasing K_{pp}^D the system is steered to a new equilibrium configuration where the two contributions compensate each other, up to instability when the derivative contribution is too big.

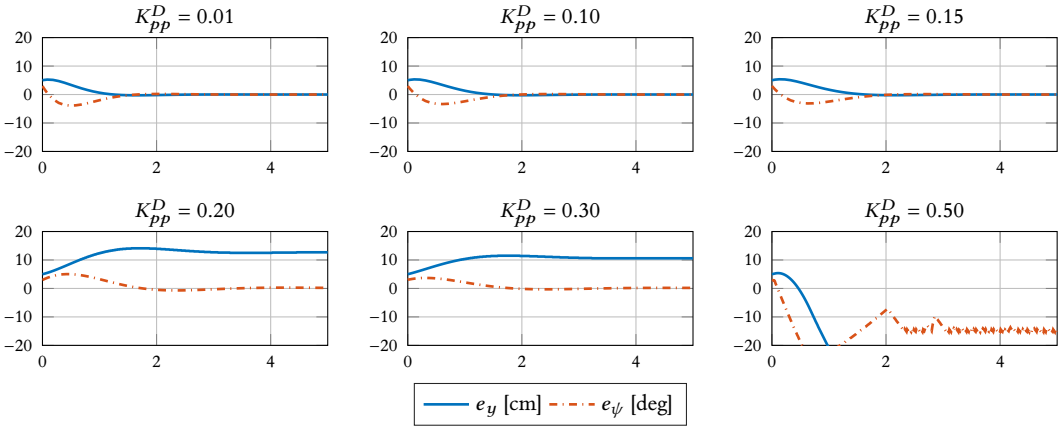

Figure 3.10: Simulation of PP-PD circular path tracking with $\rho_s = 1.04\,\text{m}$, initial condition $\mathbf{x}_0 = [0.05, 3\pi/180]$, varying K_{pp}^D for fixed $L_d = 0.5\,\text{m}$ in the delay-free case.

3.4 The PP velocity reference generation

In order to guarantee homogeneity along motion, in this section a technique for velocity reference generation based on the PP geometry is presented. The proposed technique is based on the

longitudinal control implemented in [7] and aims to drive the vehicle at a desired speed v^{MAX} avoiding excessive lateral acceleration on corners. To do so, the goal speed is defined as:

$$v = \min\left\{v^{\text{MAX}}, \sqrt{\frac{a_c^{\text{MAX}}}{\kappa(t)}}\right\} \tag{3.20}$$

where $\kappa(t)$ is the curvature of the road and $a_c = {}^{v^2}/_R = v^2\kappa$ is the lateral acceleration. In [7] the current vehicle acceleration is computed so that the vehicle's velocity converges exponentially to the desired goal velocity. This approach requires to know the curvature of the path that could be estimated either from a reliable global positioning system or from the camera mounted on the vehicle. In our scenario neither of these options is available but lateral control is based on the Ackerman geometry and the PP strategy lies on the assumption that curvature between the current position and the lookahead point is constant, with the radius of the interpolated arc of circumference given by (3.1). Indeed, as discussed in [16], the basic PP control law (3.3) could be recast in order to use the lateral acceleration as control variable:

$$a_c = \frac{v^2}{R} = \frac{2v^2 \sin\alpha}{L_d} \tag{3.21}$$

The relation between the LHE and the curvature thus allows to define the speed reference as a function of the LHE, given a maximum lateral acceleration a_c^{MAX}:

$$v = \min\left\{v^{\text{MAX}}, \sqrt{\frac{L_d}{2\sin\alpha}\, a_c^{\text{MAX}}}\right\} \tag{3.22}$$

3.5 Chapter conclusions

In this chapter three strategies to augment the basic PP controller were introduced. A deeper analysis of the linearized basic PP control law highlighted the twofold nature of the lookahead distance in tuning the tradeoff between aggressiveness and accuracy, along with the velocity of the vehicle. In order to tune the aggressiveness of the tracking performance along straight paths, a proportional gain can be added to the basic PP control law. The analysis suggests to decrease the gain along with increasing velocity, keeping in mind that too small gains could result in a too slow steering action that would drive the vehicle out of lane.

This strategy showed not to hold anymore along circular sections where the proportional gain is constrained to 1 in order to guarantee zero steady-state lateral error. In this scenario, the choice of the lookahead distance plays a role in compensating for gain variations that may be present due to nonidealities of the model, with bigger lookahead distances that allow to reduce the sensitivity around the unitary equilibrium configuration. Anyway, when increasing the lookahead distance, the "cutting-corner" effect is more likely to occur and may degrade the tracking performance.

In order to reduce such behaviour, two strategies were proposed. A noiseless estimation from the CNN allowed to add a derivative action on the LHE. In the straight scenario, the PP-PD controller allows to improve both the responsiveness and the shape of the closed loop response

by acting on the proportional and derivative gains. In the circular scenario, the derivative action allows to tune tracking accuracy. Anyway, as observed in simulation, it has to be noticed that the derivative action counteracts the proportional one by its nature with too big gains that may drive the system unstable.

Eventually a velocity reference generation technique based on the Ackerman geometry was introduced to act on the anticipative action already introduced by the PP controller, by setting the velocity according to the maximum lateral acceleration in order to guarantee homogeneity along the motion.

A pure camera based controller is then proposed, based on a single data estimated from a CNN. As already seen in simulations, some care must be taken when implementing these control strategies due to the presence of nonidealities of the model, like saturation of control and state variables, that may drive the system to instability. In view of implementing the proposed controller on the real car, several factors can affect performance and stability but the main and most present is the delay in the control loop. Intuitively it is expected that the delay will degrade performance, possibly leading to instability of the control system.

CHAPTER

4 Delayed stability analysis

Unlike what happens in the real car, the analysis done so far relies upon the assumption that the steering reference acts immediately on the system.

In Sec.2.5 a model for the delay of the steering mechanism was introduced. In particular two types of actuation delay can be distinguished: the time in between when the reference signal is applied and when the steering wheel starts turning is called *steering delay*; once the wheel starts turning, the movement occurs with a certain dynamics, modelled by a first order system with time constant referred to as *steering lag*. Intuitively it is expected that the effect of combined steering lag and delay will degrade performance, possibly leading to instability of the control system.

In this Chapter a time-delay stability analysis is presented for both the straight and circular scenarios, specifically addressing the maximization of the vehicle speed. With this in mind, the *Walton-Marshall* (WM) direct method is employed as approximate tool in a numerical analysis in finding the values of static steering delay for which the system is stable for fixed control and system parameters. The WM analysis is then used to determine tuning bounds in view of an implementation on the real car. What will be proved in this Chapter is that the proposed PP-PD control action, analyzed in the previous chapter, has the effect of compensating for effects due to the presence of delay and thus allows to increase the speed of the vehicle.

4.1 The Walton-Marshall (WM) direct method

The stabilization of delay-free systems is relatively easy to study because the number of roots of their characteristic equations is finite. However, when time delays are introduced, the number of roots is no longer finite, making the establishment of stability quite a difficult task. The Hermite-Bieler Theorem for Quasi Polynomials gives necessary and sufficient conditions under which the roots of the characteristic equation of a time-delay closed loop system have negative real part [18].

Walton and Marshall in [25] presented an alternative analysis in the particular case of time-delay systems with a single delay with the following characteristic equation:

$$\Delta(s) = d(s) + n(s)e^{-s\tau_d} \tag{4.1}$$

where $d(s)$ and $n(s)$ are coprime polynomials with real coefficients, $\deg d(s) = q$, $\deg n(s) = p$, $q \geq p$ and $\tau_d > 0$ is the time delay of the system.

This method, also called *direct method*, is usually employed as approximate tool in a numerical analysis in finding the values of τ_d for which the system is stable for fixed control and system parameters [11] and is composed of three steps:

STEP 1: Examine the stability of (4.1) for $\tau_d = 0$ using classical methods and determine the number of roots, if any, of

$$\Delta(s, \tau_d) = d(s) + n(s)e^{-s\tau_d} = 0 \tag{4.2}$$

not lying in the open LHP;

STEP 2: Consider the case of infinitesimally small positive τ_d. In this case the number of roots changes from being finite to infinite. Due to the continuity property of the roots of a quasi-polynomial with respect to a strictly positive delay, for an infinitesimally small τ_d, if $q > p$, all new roots of (4.2) must lie on the LHP and this step can be omitted. The case where $p = q$ involves more details and is studied intensively in [23].

STEP 3: Find positive values of τ_d, if any, at which there are roots of (4.2) lying on the imaginary axis and then determine whether these roots merely touch the axis or whether they cross from one half plane to the other for increasing τ_d. To do so, determine the positive roots $\omega^\star$ of

$$Q(\omega^2) := d(j\omega)d(-j\omega) - n(j\omega)n(-j\omega), \tag{4.3}$$

the corresponding positive values of τ_d s.t

$$e^{-j\tau_d\omega^\star} = -\frac{d(j\omega^\star)}{n(j\omega^\star)} \tag{4.4}$$

and the nature of these roots by inspecting the derivative of the polynomial Q with respect to ω^2:

$$S = \operatorname{sign}\left[\left.\frac{\mathrm{d}Q(\omega^2)}{\mathrm{d}\omega^2}\right|_{\omega=\omega^\star}\right] = \begin{cases} +1 & \omega^\star \text{ destabilizing} \\ -1 & \omega^\star \text{ stabilizing} \end{cases} \tag{4.5}$$

If there are no repeated roots, then the stabilizing and destabilizing roots alternate.

4.2 STRAIGHT SCENARIO

As it may be depicted by the previous chapter, the straight scenario differs from the circular one by the fact of being symmetrical with respect to the reference path. In this case, the steady state lateral acceleration is zero and performance can be tuned almost arbitrarily at every velocity by resorting to the PP-PD controller. In the straight scenario, the reference path has zero curvature and the process transfer function is reported here for sake of completeness:

$$P_S(s) = \frac{v^2}{\ell L_d}\frac{1 + s\frac{L_d}{v}}{s^2}$$

4.2.1 *Proportional PP control*

According to the the first step of the WM procedure, the closed loop characteristic equation obtained by combining the PP-P controller with the system transfer function in the steering delay free case is:

$$\begin{aligned}\Delta(s) &:= d(s) + n(s)e^{-s\tau_d} \\ &= s^2(1+s\tau) + K_{pp}^P \frac{2v^2}{L_d^2}\left(1 + s\frac{L_d}{v}\right)e^{-s\tau_d} \\ &\overset{\tau_d=0}{=} \tau s^3 + s^2 + \frac{2v}{L_d}K_{pp}^P s + \frac{2v^2}{L_d^2}K_{pp}^P\end{aligned}$$

Stability of the static-delay-free system can be inspected by resorting to the Routh-Hurwitz criterion. The Routh Table for this polynomial is

3	τ	$K_{pp}^P \frac{2v}{L_d}$
2	1	$K_{pp}^P \frac{2v^2}{L_d^2}$
1	$K_{pp}^P \frac{2v}{L_d}\left(1 - \frac{v\tau}{L_d}\right)$	
0	$K_{pp}^P \frac{2v^2}{L_d^2}$	

Stability is guaranteed under the same condition found by Ollero and Heredia in [14] which entail a lower bound on the lookahead distance:

$$\begin{cases} K_{pp}^P \dfrac{2v^2}{L_d^2} > 0 \\ 1 - \dfrac{v\tau}{L_d} > 0 \end{cases} \implies \begin{cases} K_{pp} > 0 \\ L_d > v\tau \end{cases} \tag{4.6}$$

It worth to notice that, in a linearized scenario, this is equivalent to requiring for the pole introduced by the steering dynamics to lie after the zero introduced by the PP controller. In Fig.4.1 it is reported a parametric analysis on the static-delay-free system with $\tau = 0.17\,\mathrm{s}$ and fixed velocity $v = 1\,\mathrm{m\,s^{-1}}$. It can be noticed how the steering lag sets a lower bound on the lookahead distance. Such bound can't be relaxed by the introduction of the proportional gain for the reasons mentioned in the previous chapter. Along with the lower bound on the proportional gain, this constraint gives a range of possible velocities for which stability is guaranteed under fixed steering lag. Therefore, up to now the policy to increase velocity along straight paths consists of increasing the lookahead distance (at least greater than $v\tau$) while decreasing the proportional gain up to a certain value, ensuring a fast enough input dynamics to prevent the vehicle from running out of lane. Since $\deg d(s) = 3 > 1 = \deg n(s)$, the second step of the WM procedure can be skipped. The third step aims to seek, for a fixed value of K_{pp}^P, the values of τ_d that give rise to poles that lie on the imaginary axis and whether they are stabilizing or destabilizing. These poles can be determined among the positive zeros of a particular polynomial

in the unknown ω^2 and their nature can be inferred by looking at the sign the derivative of this particular polynomial assumes in these roots.

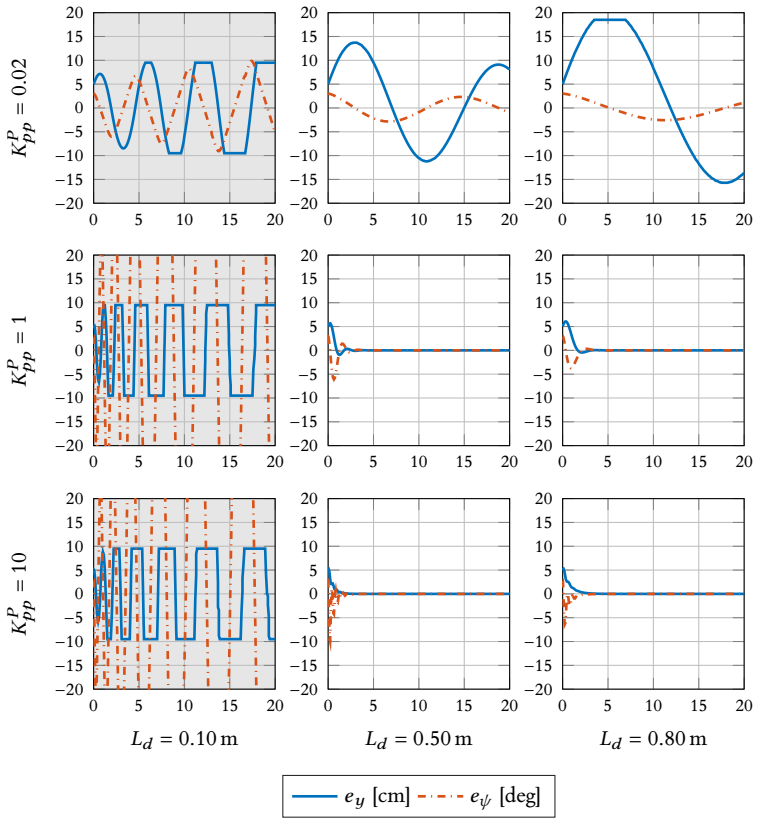

Figure 4.1: Simulation of PP-P path tracking in the straight scenario for varying K_{pp}^P and L_d and fixed $v = 1\,\mathrm{m\,s^{-1}}$.

The WM polynomial $Q(\omega^2)$, give the substitution $\eta = \omega^2$, can be derived as::

$$\begin{aligned} Q(\eta) &:= d(j\omega)d(-j\omega) - n(j\omega)n(-j\omega) \\ &= \eta^2\left(1 + \eta\tau^2\right) - K_{pp}^P \frac{4v^4}{L_d^4}\left(1 + \eta\frac{L_d^2}{v^2}\right) \\ &= \tau^2\,\eta^3 + \eta^2 - {K_{pp}^P}^2 \frac{4v^2}{L_d^2}\,\eta - {K_{pp}^P}^2 \frac{4v^4}{L_d^4} \end{aligned}$$

Its derivative with respect to η can be computed easily as:

$$\frac{\mathrm{d}Q}{\mathrm{d}\eta} = 3\tau^2\,\eta^2 + 2\,\eta - {K_{pp}^P}^2 \frac{4v^2}{L_d^2} \tag{4.7}$$

In Fig.4.2 it is plotted the critical static delay τ_d, above which the system becomes unstable as a function of the proportional gain for fixed lookahead distance of $L_d = 0.5\,\mathrm{m}$ and varying velocity.

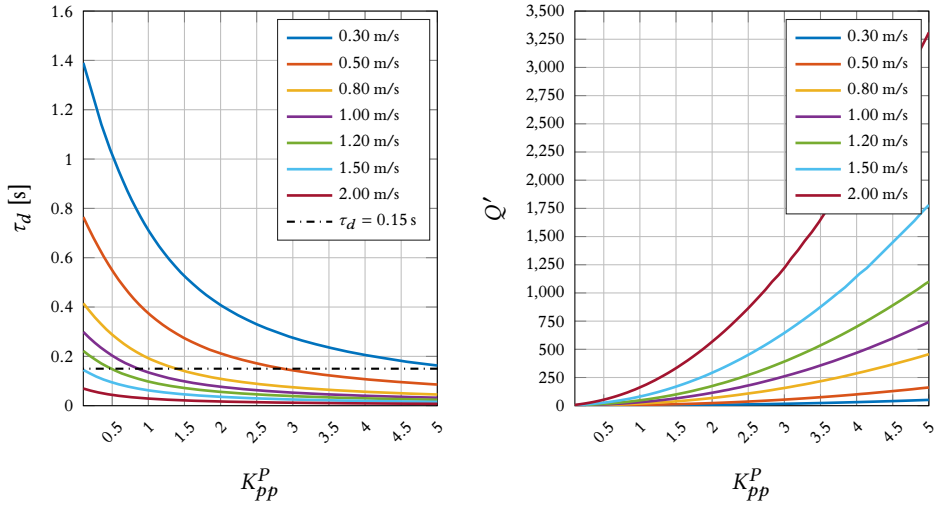

Figure 4.2: Critical τ_d as a function of the PP-P gain in the straight scenario with $L_d = 0.5$ m. On the right is the derivative of the WM polynomial.

It can be noticed that, for unitary gain, the system is unstable for 1.0 and 2.0 m s^{-1}. As velocity decreases, the upper bound for the gain increases thus letting room for tuning the shape of the response in terms of suitable performance indexes. This analysis verifies that, if $K^P_{pp} = 1$ with fixed L_d, the maximum velocity is limited by the actuation delay. Indeed, τ_d seconds are needed for a steering reference command to act on the steering mechanism and about $t_r = 2.2\tau$ seconds are needed for the wheels to perform a complete steering maneuver. If $\tau = 0.17$ s, $\tau_d = 0.15$ s and $v = 1$ m s^{-1}, the vehicle has driven 0.524 m $> L_d$ until when the steering reference is set. This suggests to increase the lookahead distance: in Fig.4.3 the same analysis is reported for $L_d = 0.8$ m. In this case curves are shifted upwards thus increasing the upper bound for the velocity for fixed gain. It's interesting to notice that in this case lowering the gain has a similar effect to increasing the lookahead distance.

4.2.2 *Proportional Derivative PP control*

Introducing the PP-PD derivative control law, the characteristic equation of the linearized feedback system becomes:

$$\begin{aligned}\Delta(s) &:= d(s) + n(s)e^{-s\tau_d} \\ &= s^2(1+s\tau) + \left(K^P_{pp}\frac{2\ell}{L_d} + sK^D_{pp}\right)\frac{v^2}{\ell L_d}\left(1 + s\frac{L_d}{v}\right)e^{-s\tau_d} \\ &\overset{\tau_d=0}{=} \tau s^3 + \left(1 + \frac{v}{\ell}K^D_{pp}\right)s^2 + \left(\frac{2v}{L_d}K^P_{pp} + \frac{v^2}{\ell L_d}K^D_{pp}\right)s + \frac{2v^2}{L_d^2}K^P_{pp}\end{aligned}$$

The Routh table in the delay free case is:

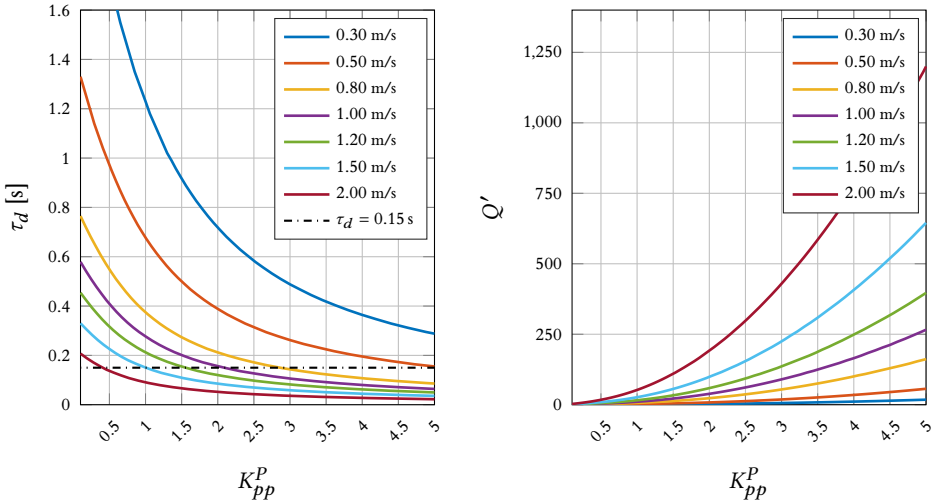

Figure 4.3: Critical τ_d as a function of the PP-P gain in the straight scenario with $L_d = 0.8$ m. On the right is the derivative of the WM polynomial.

$$
\begin{array}{c|cc}
3 & \tau & \frac{v}{L_d}\left(K^{P\star}_{pp} + K^{D\star}_{pp}\right) \\
2 & 1 + K^{D\star}_{pp} & \frac{v^2}{L_d^2} K^{P\star}_{pp} \\
1 & \frac{\frac{v}{L_d}\left[\left(K^{P\star}_{pp}+K^{D\star}_{pp}\right)\left(1+K^{D\star}_{pp}\right)-\frac{v}{\tau L_d}K^{P\star}_{pp}\right]}{1+K^{D\star}_{pp}} & \\
0 & \frac{v^2}{L_d^2} K^{P\star}_{pp} &
\end{array}
$$

where for sake of clarity $K^{P\star}_{pp} = 2K^P_{pp}$ and $K^{D\star}_{pp} = K^D_{pp}\frac{v}{\ell}$.
Besides the assumption that the PP-PD controller must introduce a stable zero, i.e. $K^P_{pp} > 0$ and $K^D_{pp} > 0$, the Routh-Hurwitz criterion yields the following conditions:

$$
\begin{cases}
\dfrac{\frac{v}{L_d}\left[\left(K^{P\star}_{pp} + K^{D\star}_{pp}\right)\left(1 + K^{D\star}_{pp}\right) - \frac{v}{\tau L_d}K^{P\star}_{pp}\right]}{1 + K^{D\star}_{pp}} > 0 \\
\frac{v^2}{L_d^2} K^{P\star}_{pp} > 0
\end{cases}
\quad \Longrightarrow \quad
\begin{cases}
L_d > \underbrace{\left(\dfrac{K^{P\star}_{pp}}{\left(K^{P\star}_{pp} + K^{D\star}_{pp}\right)\left(1 + K^{D\star}_{pp}\right)}\right)}_{\mu(K^P_{pp}, K^D_{pp})} v\tau \\
K^P_{pp} > 0
\end{cases}
$$

The first constraint is now modified by the derivative gain with an added term $\mu(K^P_{pp}, K^D_{pp})$ that depends on both the proportional gain, the derivative gain and the ratio between the velocity and the wheelbase distance. Fig.4.4 illustrates this function for positive values of the gains: it can be noticed how this function is upper bounded by the null-derivative-gain-case, in which the

constraint is the same as in (4.6). As the derivative gain increases, for fixed proportional gain, the bound on the L_d is relaxed, thus enabling to increase the speed for fixed lookahead distance.

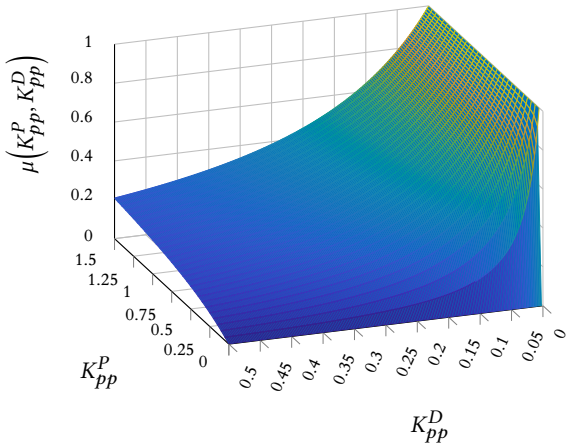

Figure 4.4: Function $\mu(K_{pp}^P, K_{pp}^D)$ with $\ell = 0.26\,\mathrm{m}$ and fixed $v = 1\,\mathrm{m\,s^{-1}}$

The WM polynomial $Q(\eta)$ has two degrees of freedom in the proportional and derivative gains and is expressed by:

$$\begin{aligned} Q(\eta) &:= d(j\omega)d(-j\omega) - n(j\omega)n(-j\omega) \\ &= \eta^2\left(1+\eta\tau^2\right) - \frac{4v^4}{\ell^2 L_d^2}\left[\left(K_{pp}^{P\,2}\frac{4\ell^2}{L_d^2} + K_{pp}^{D\,2}\eta\right)\left(1+\eta\frac{L_d^2}{v^2}\right)\right] \\ &= \tau^2\,\eta^3 + \left(1 - K_{pp}^{D\,2}\frac{v^2}{\ell^2}\right)\eta^2 - \left(K_{pp}^{P\,2}\frac{4v^2}{L_d^2} + K_{pp}^{D\,2}\frac{v^4}{\ell^2 L_d^2}\right)\eta - K_{pp}^{P\,2}\frac{4v^4}{L_d^4} \end{aligned} \tag{4.8}$$

With derivative:

$$\frac{\mathrm{d}Q}{\mathrm{d}\eta} = 3\tau^2\,\eta^2 + 2\left(1 - K_{pp}^D\frac{v^2}{\ell^2}\right)\eta - \left(K_{pp}^{P\,2}\frac{4v^2}{L_d^2} + K_{pp}^{D\,2}\frac{v^4}{\ell^2 L_d^2}\right) \tag{4.9}$$

Fig.4.5 illustrates the 3D plot of the critical delay as a function of both K_{pp}^P and K_{pp}^D for increasing velocity and a slice of this plot corresponding to the value $K_{pp}^P = 1$: it can be noticed how, for a fixed value of K_{pp}^P, there exists a K_{pp}^D that yields the maximum critical delay which, for increasing the velocity, tends to converge to a value in the interval $[0.10, 0.15]$. Moreover, as expected, decreasing K_{pp}^P has the effect of strengthening stability for increasing velocities. Moreover adding too much derivative action has the same effect as having no derivative contribution at all in terms of stability. In view of an implementation in the real car, this analysis gives also an order of magnitude for tuning the PP-PD controller.

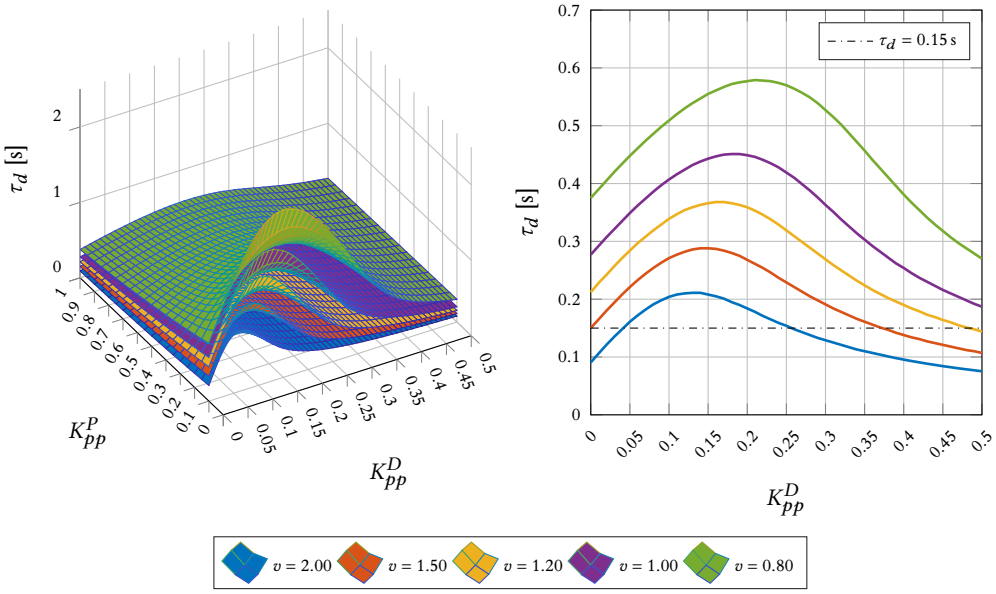

Figure 4.5: Critical τ_d as a function of the PP-PD gains in the straight scenario with $L_d = 0.8$ m. On the right a slice corresponding to $K^P_{pp} = 1$

4.3 Circular scenario

In the circular scenario the DoF introduced by the proportional gain is no more available due to zero steady-state tracking purposes. In the previous Chapter, this constraint motivated the introduction of a derivative action on the LHE and a PP-based velocity reference generation technique in order to tune the anticipative action of the controller. Since in this case the WM analysis can't be applied on control parameters, the path radius will be considered as a varying system parameter. The process transfer function is reported here for sake of completeness:

$$P_C(s) = C_c[sI - A_c]^{-1}B_c = \frac{v^2\lambda\gamma}{\ell}\frac{1 + s\frac{1}{v\lambda}}{s^2 + \frac{v^2}{{\rho_s}^2}}$$

4.3.1 *Proportional PP control*

The the closed loop characteristic equation obtained by combining the basic PP controller with the transfer function of the process is:

$$\begin{aligned}\Delta(s) &:= d(s) + n(s)e^{-s\tau_d} \\ &= \left(s^2 + \frac{v^2}{{\rho_s}^2}\right)(1 + s\tau) + \frac{2v^2\gamma\lambda}{L_d}\left(1 + s\frac{1}{v\lambda}\right)e^{-s\tau_d} \\ &\overset{\tau_d=0}{=} \tau s^3 + s^2 + \left(\frac{v^2\tau}{{\rho_s}^2} + \frac{2v^2\gamma}{L_d}\right)s + \frac{v^2}{{\rho_s}^2} + \frac{2v\gamma\lambda}{L_d}\end{aligned}$$

The Routh-Hurwitz criterion applied on the Routh Table in the steering delay free case:

$$\begin{array}{c|cc} 3 & \tau & \frac{v^2\tau}{{\rho_s}^2} + \frac{2v^2\gamma}{L_d} \\ 2 & 1 & \frac{v^2}{{\rho_s}^2} + \frac{2v\gamma\lambda}{L_d} \\ 1 & \frac{2v\gamma}{L_d}(1 - v\lambda\tau) & \\ 0 & \frac{v^2}{{\rho_s}^2} + \frac{2v\gamma\lambda}{L_d} & \end{array}$$

yields the following conditions:

$$\begin{cases} \frac{v^2}{{\rho_s}^2} + \frac{2v\gamma\lambda}{L_d} > 0 \\ 1 - v\lambda\tau > 0 \end{cases} \implies \begin{cases} \lambda > -\frac{vL_d}{2\gamma{\rho_s}^2} \\ \lambda^{-1} > v\tau \end{cases}$$

If $\rho_s > L_d$, then the first inequality is always verified, while the second resembles the constraint for the lookahead distance found in the straight case (4.6). In Fig.4.6 the parameter λ^{-1} is plotted as a function of the path radius ρ_s. As expected, as $\rho_s \to \infty$, the reciprocal of λ tends to the lookahead distance L_d. Here it can be noticed how, without static delay, if the system is stable in the straight case, it remains so when the vehicle is approaching and is inside a curve. It could also happen, for a certain velocity, that the system is unstable in the straight case and becomes stable when entering a curve.

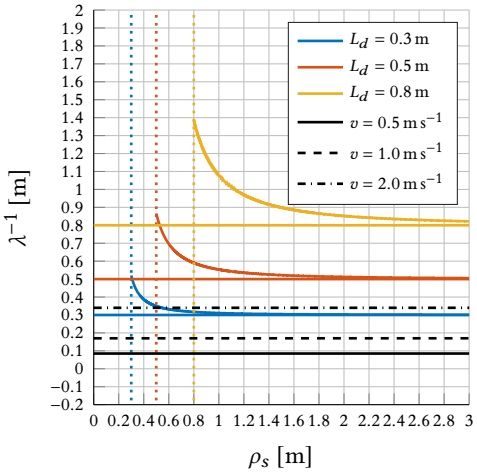

Figure 4.6: Parameter λ as a function of the path radius $\rho_s > L_d$. The horizontal asymptote is $\lambda^{-1} = L_d$. Black levels represent the product $v\tau$ for different velocities.

In figure 4.7 it is reported the critic static delay as a function of the path radius for varying velocity . As $\rho_s \to L_d$, the shape of the critic delay resembles the one of the parameter λ in the case with lag and no delay, slightly bending upwards. It can be verified that, as $\rho_s \to \infty$, critic delay levels tends to the values with unitary gains in the straight case and it can be concluded

that, even if stability is reinforced as path curvature increases, the improvement with respect to the straight case is negligible.

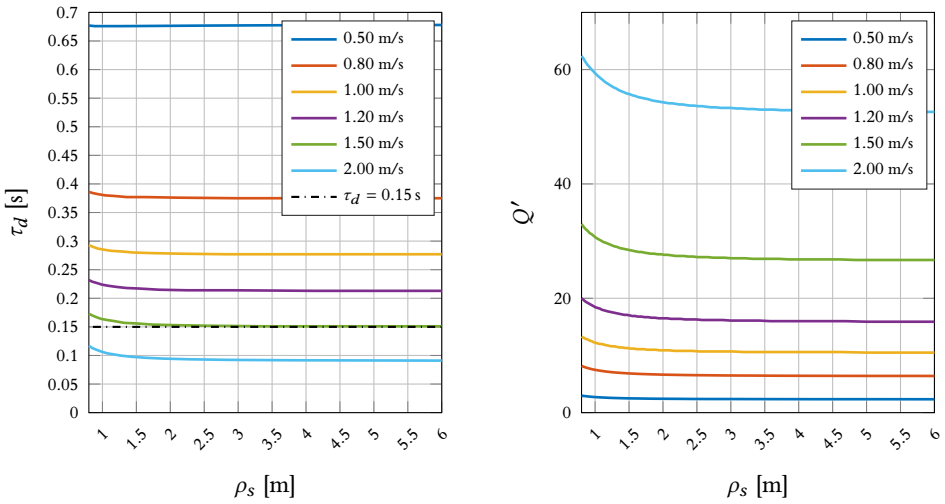

Figure 4.7: Critical τ_d as a function of the path radius gain in the circular scenario with $L_d = 0.8$ m. On the right is the derivative of the WM polynomial.

4.3.2 *Proportional Derivative PP control*

Without going into details on computations, in this case a qualitative analysis on the 3D plot reported in Fig.4.8 will be presented. The WM polynomial in this case is:

$$
\begin{aligned}
Q(\eta) &:= d(j\omega)d(-j\omega) - n(j\omega)n(-j\omega) \\
&= \left(\frac{v^2}{{\rho_s}^2} - \eta\right)^2 \left(1 + \eta\tau^2\right) - \frac{v^4\lambda^2\gamma^2}{\ell^2}\left[\left(\frac{4\ell^2}{L_d^2} + {K_{pp}^D}^2\eta\right)\left(1 + \frac{\eta}{v^2\lambda^2}\right)\right] \\
&= \tau\eta^3 + \left(1 - \frac{2v^2\tau^2}{{\rho_s}^2} - \frac{v^2\gamma^2{K_{pp}^D}^2}{\ell^2}\right)\eta^2 + \left(-\frac{2v^2}{{\rho_s}^2} + \frac{v^4\tau^2}{{\rho_s}^4} - \frac{4v^2\gamma^2}{L_d^2} - \frac{v^4\lambda^2\gamma^2{K_{pp}^D}^2}{\ell^2}\right)\eta + \cdots \\
&\quad \cdots + \left(\frac{v^4}{{\rho_s}^4} - \frac{4v^4\lambda^2\gamma^2}{L_d^2}\right)
\end{aligned}
$$

As in the proportional case, K_{pp}^P is constrained to be equal to 1 so the path radius can be treated as a varying system parameter. From the shape of the surfaces it is clear that the effect of the derivative action remains the same in the circular case for fixed proportional gain and path curvature. As the path radius decreases, the surfaces bend downwards thus degrading stability. This reasoning is in line with the analysis done in the previous chapter and suggests,for a fixed derivative gain, to decrease the speed as path curvature increases.

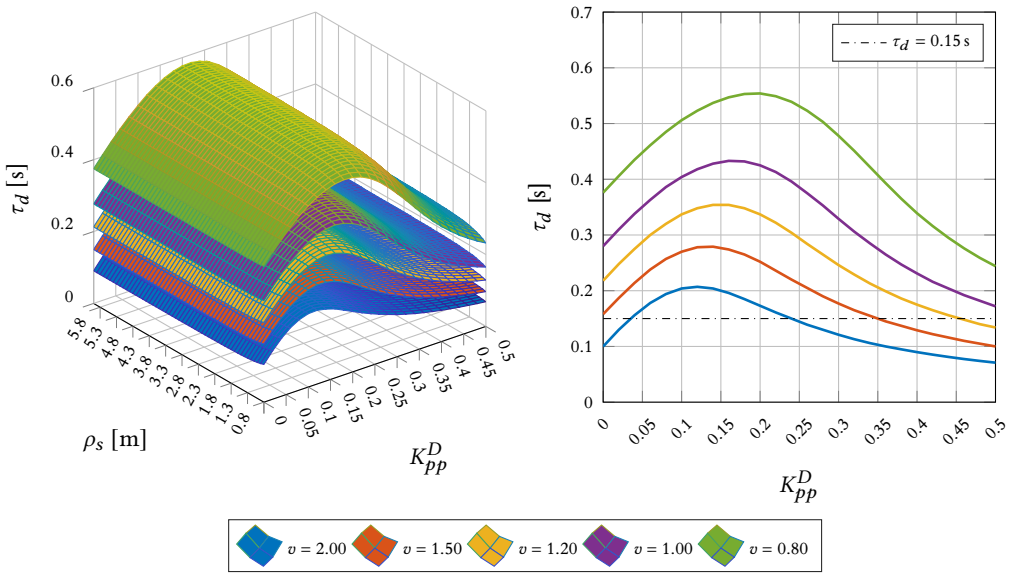

Figure 4.8: Critical τ_d as a function of the derivative gain for fixed $K^P_{pp} = 1$ in the circular scenario with $L_d = 0.8$ m and $\rho_s = 1.04$ m.

4.4 Chapter conclusions

In this chapter a thorough analysis of stability in the presence of the steering actuation dynamics was presented on the linearized feedback control system.
Starting from the straight scenario, the introduction of the steering lag leads to a lower bound on the lookahead distance that, besides lag, depends also on velocity. This first condition allows to define a subset of stable velocities for fixed lookahead distance and steering lag. The bound on the lookahead distance can't be relaxed by the introduction of the proportional gain which itself enables to shape the response of the system and trades performance between the heading and the lateral error responses. Considering also the steering delay in the model has the effect of shrinking the space of stable velocities for fixed lookahead distance and introduces an upper bound on the proportional gain. In order to increase the range of stable velocities, two strategies can be adopted: either the lookahead distance is increased or the proportional gain is decreased, still keeping in mind the nonidealities of the model that may drive the system unstable.
In the circular scenario, the proportional gain is constrained to 1 but in this case the bound introduced by the steering lag is shown to relax as curvature increases. Also in this case the introduction of the steering delay has the effect of shrinking the space of stable velocities but no strategy can be adopted to counteract this fact due to the missing degree of freedom on the proportional gain. Then, the derivative action is introduced and the time-delay analysis showed a maximum critical delay as a function of the derivative gain in both the straight and circular cases, for both fixed lookahead distance and proportional gain. Moreover, in the circular scenario, stability is observed to degrade as the curvature of the path increases, therefore suggesting to decrease velocity as approaching a curve.

CHAPTER

5 Results

In this Chapter, results coming from the implementation of the controllers described above are discussed, specifically addressing performance evaluation on a reference test track in a laboratory environment. In Sec.5.1 the setup of the BFMC car is described in detail. In this scenario, the Lookahead Heading Error (LHE) — input to the PP-based controller — is retrieved by a Convolutional Neural Network (CNN) which is trained by means of a Gazebo simulator. The trained model is used to compute the LHE from images with a resolution of 320×240 px coming from a RasPi Camera V2 module mounted on top of the car. Reference control signals are applied to the actuators through a STM32 Nucleo board: the steering angle reference is applied to a DC servomotor through a square wave signal with variable duty cycle and the desired speed is set as reference of an inner loop with a PID controller that drives a DC motor through feedback from an encoder mounted on its shaft.
Three results are then presented: in Sec.5.3 the control behaviour of the basic PP control law is verified exploiting the exact feedback from a motion capture system; the effect on tracking performance by varying the proportional gain is observed in Sec.5.4; eventually, tracking performance of the proposed PP-PD + PP-based velocity reference generation technique is evaluated in Sec.5.5 by means of suitable metrics.

5.1 Physical setup

The 1:10 vehicle used for validating the controller, shown in Fig.5.1, comes from the participation of the DEI-Unipd Team in the Bosch Future Mobility Challenge.
It is a 1:10 scale vehicle with wheelbase distance $\ell = 0.26$ m equipped with two control boards: namely a Raspberry Pi (RPi) ① and a STM32L476RG Nucleo board ②. Above the car a RasPi Camera V2 ③ module is fixed at the same pose of the camera in the Gazebo simulator and is connected to the RPi where images are acquired with a resolution of 640×380 pixels at 30 FPS. Three HC-SR04 ultrasonic sensors ④ on the front side and one on the right side are placed and connected to the Raspberry Pi in order to detect obstacles, pedestrians and parked cars. The actuation part is handled by the Nucleo board which forwards speed and steer commands from the RPi to a DC motor ⑤ through a power driver and to a DC servomotor ⑥ for steering. The estimated static delay is $\tau_d = 0.15$ s and the steering lag time constant is $\tau \approx {}^{t_r}/_{2.2} = 0.17$ s, where t_r is the rise time of a complete no-load steering maneuver from $-28°$ to $28°$. The orientation of the vehicle is measured by means of a Bosch BNO055 Smart IMU sensor ⑧ connected to the RPi via I2C protocol. Speed and relative position feedbacks are retrieved by an AMT103 high accuracy incremental encoder mounted on the shaft of the DC motor. Everything is powered

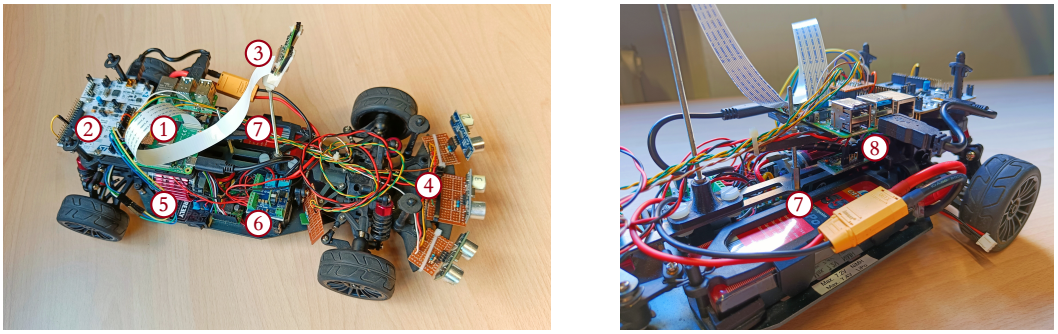

(a) Top view (b) Side view

Figure 5.1: Vehicle of the DEI-Unipd Team used for the tests in this thesis

by a Li-Ion battery pack ⑦ placed on the lower left side, interfaced with perhiperals through a DC-DC converter. Autonomous tasks are orchestrated by a state machine in the RPi coded in Python, while the Nucleo board, coded in C++, acts as a ROS node within a ROS network: UART serial communication with the RPi is managed inside the Nucleo by Direct Memory Access and ROSserial interface.

5.2 Testing scenario

The applicability of the control laws described in previous chapters have been tested on a custom made track inside the SPARCS laboratory at the Department of Information Engineering at the University of Padua. The scenario in which the controllers have been evaluated consists of a test track traced on an anti-slip material of dimensions 3×6 m surrounded by a VICON MoCap system allowing for motion tracking of the car pose.
The reference track is composed of two straight sections of length L, a bigger 180-degree curve of radius R and two smaller 90-degree curves of radius r joined by a straight section, with parameters reported in Tab.5.1. Under the assumptions (a) $r < R$ and (b) $R_e + m < x_c$, the test track is partitioned into parametrized sections:

$$\left\{ \mathbf{r}_{ij} \in \mathbb{R}^2 \,\middle|\, 1 \leq i \leq 6, j = (i+1) \bmod 6 \right\}$$

such that:

$$\mathbf{r}_{12}(\theta) = \begin{bmatrix} x_c + R\cos\theta \\ (m + R_c) + R\sin\theta \end{bmatrix} \qquad \theta \in [0, -\pi]$$

$$\mathbf{r}_{23}(\lambda) = \begin{bmatrix} x_c - R \\ \lambda(m + R_c) + (1-\lambda)(m + R_c + L) \end{bmatrix} \qquad \lambda \in [0, 1]$$

$$\mathbf{r}_{34}(\theta) = \begin{bmatrix} (x_c - R + r) + r\cos\theta \\ (m + R_c + L) + r\sin\theta \end{bmatrix} \qquad \theta \in \left[-\frac{\pi}{2}, -\frac{3\pi}{2} \right]$$

Sym	Description	Value
x_c	Abscissa of the axis of symmetry of the path	1.5 m
m	Margin between the path and the edge of the fabric	0.25 m
R_c	Bigger radius of the lane center	1.04 m
w	Lane width	0.37 m
R_i, R_e	Internal and external bigger radii of the track	$R_c - \frac{w}{2}, R_c + \frac{w}{2}$
r_c	Smaller radius of the lane center	0.65 m
r_i, r_e	Internal and external smaller radii of the track	$r_c - \frac{w}{2}, r_c + \frac{w}{2}$
L	Length of the straight section	2 m

Table 5.1: Parameters of the test track

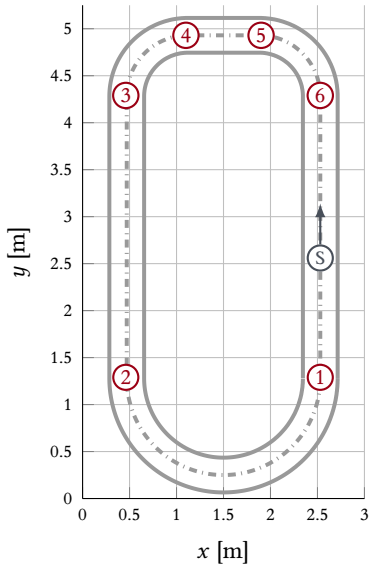

Figure 5.2: Test track parametrization. All the following tests are performed recording a lap starting from Ⓢ in counterclockwise direction.

$$\mathbf{r}_{45}(\lambda) = \begin{bmatrix} \lambda(x_c - R + r) + (1-\lambda)(x_c + R - r) \\ m + R_c + L + r \end{bmatrix} \qquad \lambda \in [0, 1]$$

$$\mathbf{r}_{56}(\theta) = \begin{bmatrix} (x_c + R - r) + r\cos\theta \\ (m + R_c + L) + r\sin\theta \end{bmatrix} \qquad \theta \in \left[-\frac{3\pi}{2}, -2\pi\right]$$

$$\mathbf{r}_{61}(\lambda) = \begin{bmatrix} x_c + R \\ \lambda(m + R_c + L) + (1-\lambda)(m + R_c) \end{bmatrix} \qquad \lambda \in [0, 1]$$

5.3 Basic PP with feedback from VICON

First of all the control behaviour of the basic PP action is verified as a function of the lookahead distance and velocity with exact feedback from the motion capture system using the relation (2.11).

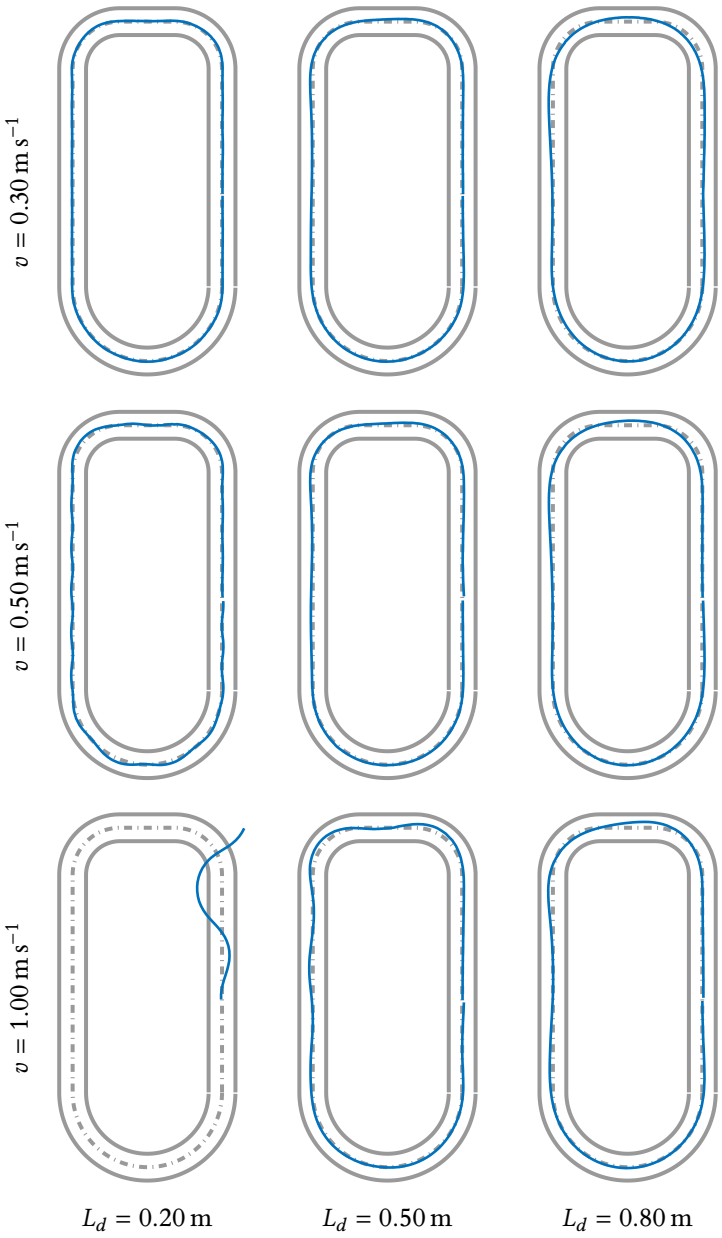

Figure 5.3: Basic PP control (3.3) with feedback from VICON and constant speed.

Fig.5.3 compares one lap per configuration in a grid pattern. These first results provide evidence to the effectiveness of such controller in tracking a given path as long as both velocity and lookahead distance are kept small. As velocity increases, increasing the lookahead allows to ensure stability at the price of an accentuated "cutting-corner" effect in tight curves and an increasingly present oscillatory behaviour triggered by the overshoot at curve exits. Scanning the grid left-right highlights the "cutting-corner" effect due to the increasing lookahead distance (top right corner) while scanning it top-down shows the effect of the steering delay in the overshoot at curve exits (bottom right corner). A diagonal upper-right to lower-left scan goes with increasing v/L_d ratio yielding increasingly oscillatory behaviours up to instability in the extreme case of $v = 1.00\,\mathrm{m\,s^{-1}}$ and $L_d = 0.20\,\mathrm{m}$. In line with previous analysis, all the stable configurations fulfill perfect tracking of the bigger curve regardless of the lookahead distance. Almost perfect tracking is achieved in the upper left corner where velocity is small, delay is negligible and the "cutting-corner" effect is almost absent due to the small lookahead distance. The results confirm that a trade-off between velocity and tracking performance must be faced so, for the BFMC technical challenge, the configuration with $v = 0.3\,\mathrm{m\,s^{-1}}$ and $L_d = 0.5\,\mathrm{m}$ with feedback from the camera (see Fig.5.4) was chosen as a good compromise between robustness and performance.

5.4 Effect of the proportional gain

The second result verifies the range of applicability of the PP-P controller discussed in Chapter 3 in a slow-speed scenario. The effect of a proportional gain in front of the basic PP control law (3.8) can be observed in Fig.5.4. The results now provide evidence to the two main aspects of the PP-P controller. Firstly, the variation of the proportional gain has no effect on steady state errors along straight sections. Secondly, a proportional gain $K_{pp}^P > 1$ along sections with non null path curvature has the effect of shifting the equilibrium towards the center of the curve. This latter behaviour may lead the vehicle to cut tight curves resulting in the camera FoV loosing the lane and eventually leading the vehicle to run off the road. Indeed the VICON case delivers significantly better results as it can be depicted in the LHE signals below: from the second tight curve the CNN couldn't estimate the correct LHE and this led to a persistent oscillatory behaviour until the end of the lap.

5.5 Speed performance

Before discussing further results, it is important to note that this section relies on the availability of two different models of the CNN that allow to obtain an estimate of the LHE at, respectively, $L_d = 0.5\,\mathrm{m}$ and $L_d = 0.8\,\mathrm{m}$. With reference to the proposed PP-PD controller, during the following experiments, the proportional gain was fixed to 1 in order to guarantee zero steady-state tracking error in curve. In order to guarantee homogeneity of travel with the aim of maximizing speed, the proposed PP-based velocity reference generation technique was adopted with a maximum speed of $1\,\mathrm{m\,s^{-1}}$. As it can be depicted in Fig.5.3, performance along tight curves at constant velocity $v = 1\,\mathrm{m\,s^{-1}}$ with $L_d = 0.8\,\mathrm{m}$ and feedback from VICON already shows a non-negligible overshoot at curve exits. Indeed this configuration becomes unstable in

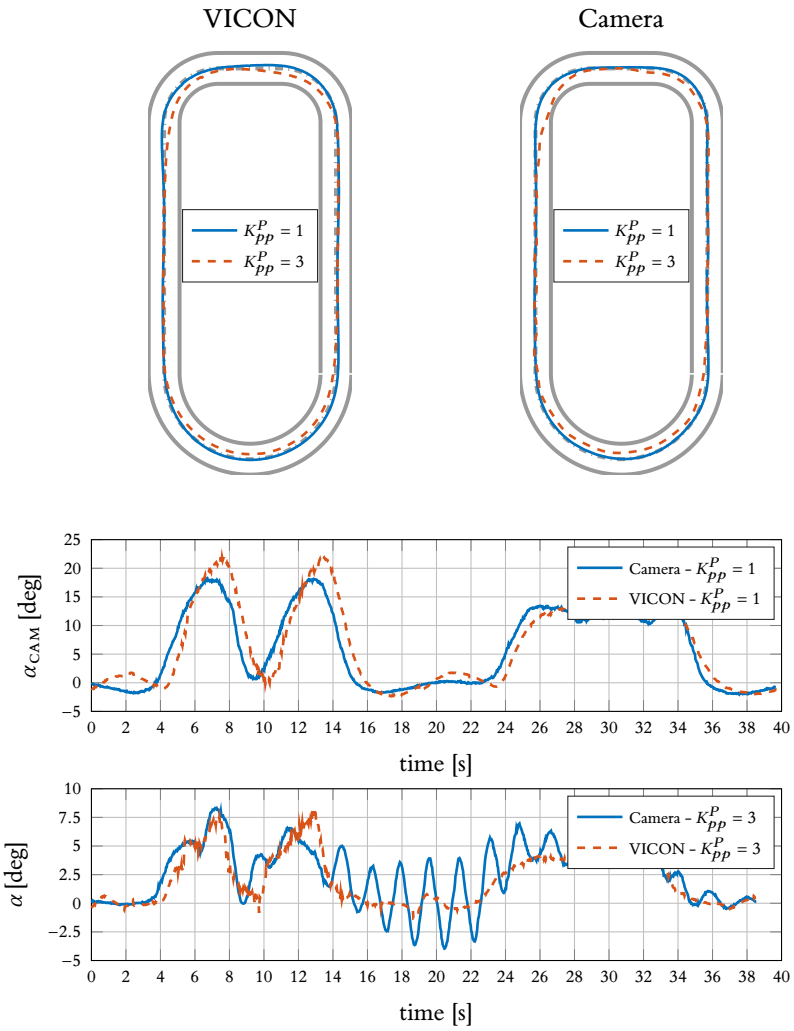

Figure 5.4: PP-P control (3.8) with constant speed $v = 0.3\,\mathrm{m\,s^{-1}}$, feedback from VICON (left) and from camera (right)

the camera-based approach where, if both the lateral and the heading error become too big, the lane exceeds the camera FOV and the CNN can't give a correct estimation of the LHE anymore. This first result highlights the need for decreasing the lookahead distance. In line with the previous analysis, decreasing L_d to 0.5 m should go along with the arise of an oscillatory behaviour due to the presence of delay in the steering actuation mechanism. In fact, as it can be noticed in Fig.5.5, even in the case with a larger lookahead distance such oscillations occur after being triggered by the overshoot at curve exits. In line with the previous analysis, these results justify the need for the introduction of the derivative action.

Planned experiments provided evidence of the previous stability analysis and also cast a new light on tracking performance. In order to evaluate performance, the following indexes on the

lateral and heading errors were used [19]:

$$e_y^{\text{MAX}} = \max_{t\in[0,T]} \left|e_y(t)\right| \qquad \text{MAXIMUM LATERAL ERROR}$$

$$e_\psi^{\text{MAX}} = \max_{t\in[0,T]} \left|e_\psi(t)\right| \qquad \text{MAXIMUM HEADING ERROR}$$

In Fig.5.7, these indexes, along with other relevant quantities, are plotted with reference to the configurations reported in Fig.5.5, with the *best result* being represented by the first configuration of Fig.5.5. Clearly the first configuration outperforms the others by means of both maximum lateral and heading errors, thus providing a more concentrated distribution of the lateral error magnitude. Anyway, as expected, the damping nature of the derivative action degrades the aggressiveness of the control action. Indeed, as it can be depicted in Fig.5.6, the distribution of the magnitude of the lateral error in the best case is slightly skewed. In order to avoid it, one could act on the proportional gain and on its ratio with the derivative one along straight sections as described in Sec.3.3.1. Planned comparisons reveal the effectiveness of the proposed derivative action in damping oscillations. Besides the best case, this behaviour can be noticed also in the comparison between the second and third scenarios with $L_d = 0.8\,\text{m}$. In this case, performance along the two tight curve sequence can't be improved by the introduction of the derivative action which, on the other hand, allows to improve robustness after the second tight curve, along the straight section and after the fast curve, where it significantly reduces the overshoot.

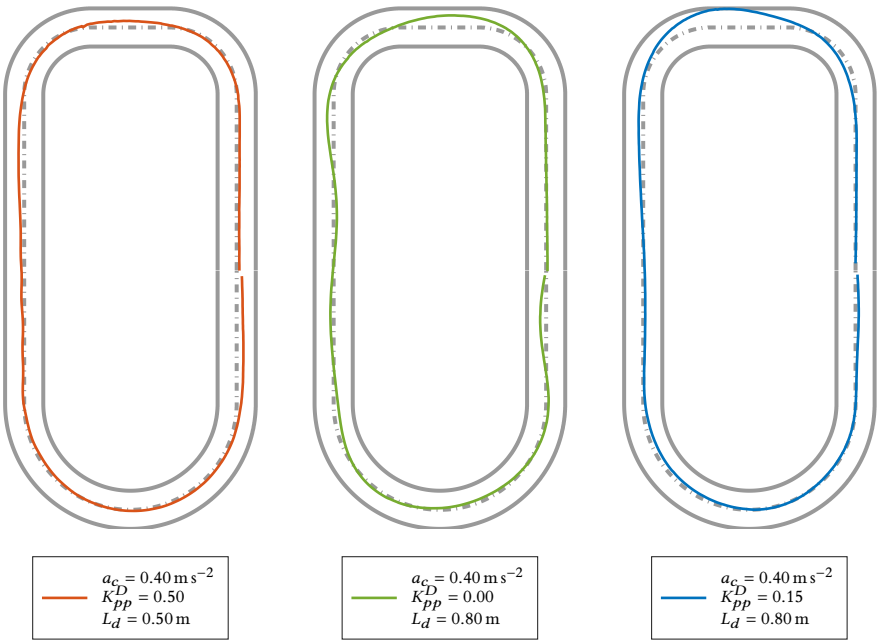

Figure 5.5: PP-PD control with feedback from camera and PP based velocity reference generation. The first on the left represents the best result on the test track. In particular it can be noticed the effectiveness of the derivative action in damping oscillations and overshoots at curve exits. The derivative action in the third configuration leads to a peak after the second tight curve but allows to perform better than the second in the second half of the track.

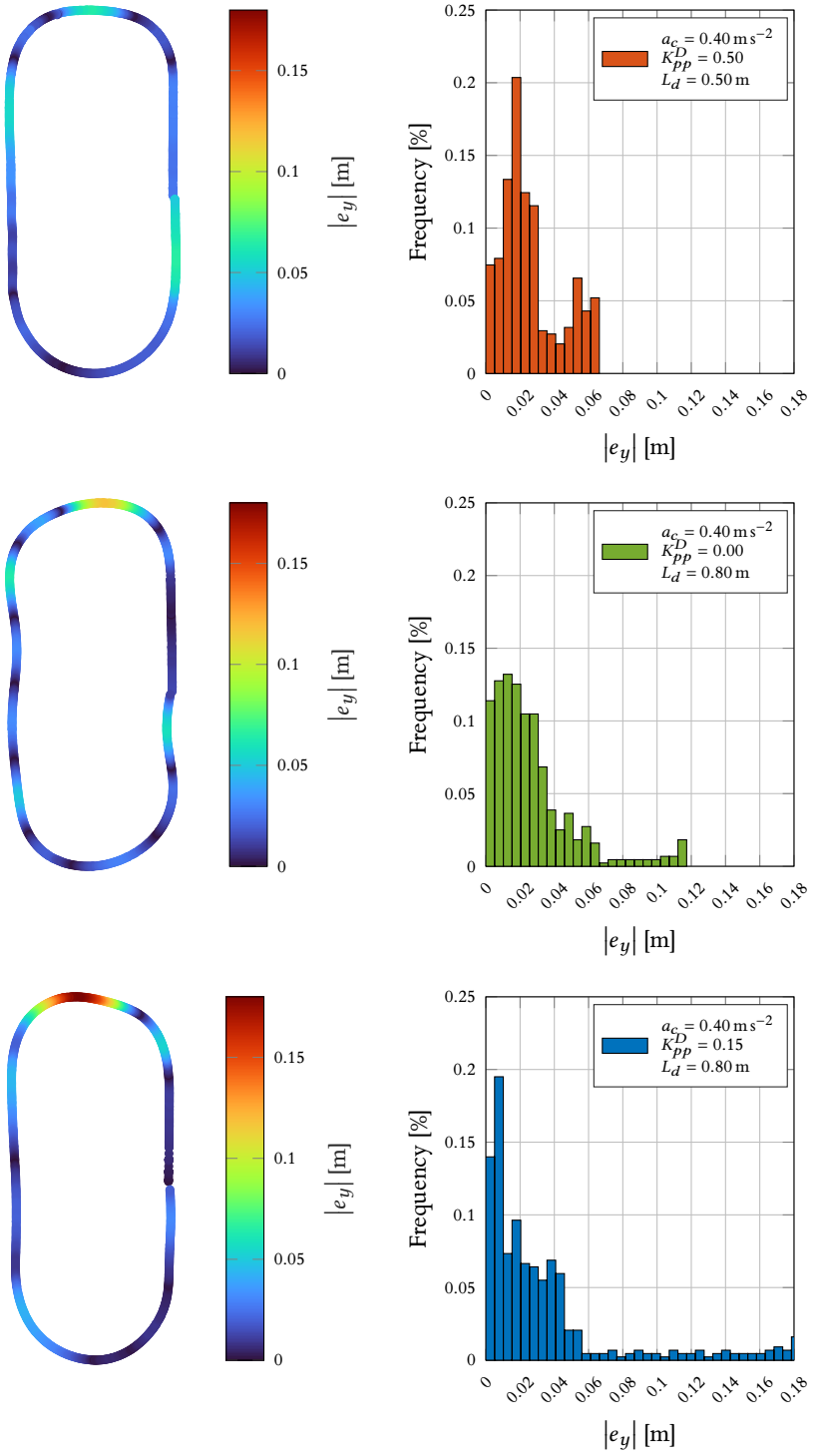

Figure 5.6: Distribution of the lateral error magnitude computed on the configurations in Fig.5.5. Even if the best configuration shows the most concentrated distribution, a little skewness is caused by the derivative action. The oscillatory behaviour in the second configuration is well represented by a wider distribution.

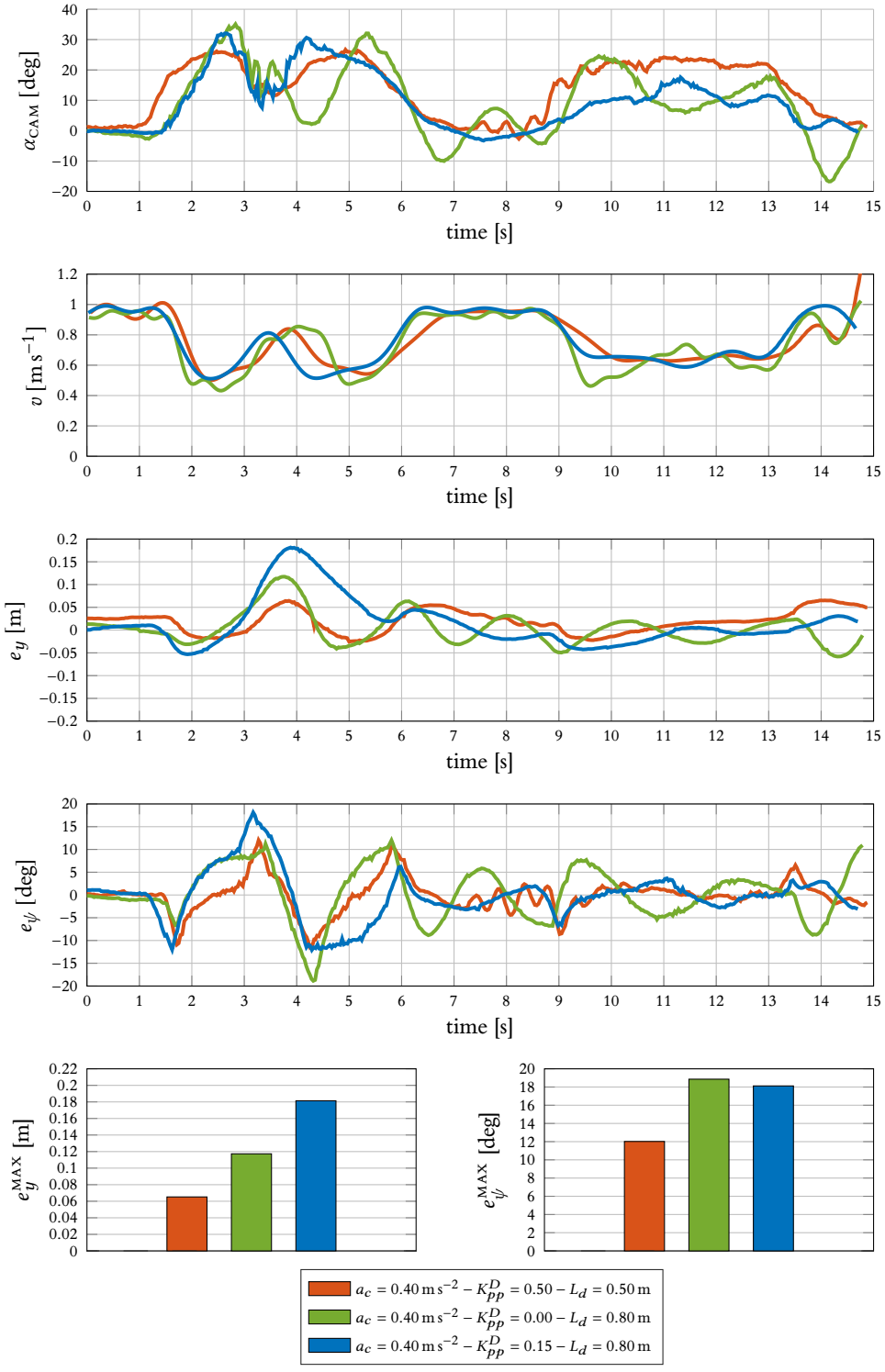

Figure 5.7: Performance metrics and useful quantities referred to the laps in Fig.5.5. The best performance of the fist configuration can be noticed comparing the velocity profile generated by the proposed PP-based technique and the metrics evaluation on the lateral and heading errors.

CHAPTER

6 Conclusions

In this thesis a pure pursuit lane keeping controller for a 1:10 scale vehicle was proposed, specifically addressing the maximization of the vehicle speed, along with ensuring good tracking performance in the framework of the BFMC 2022.
In this limited scenario, the only available data, namely the Lookahead Heading Error - input to the PP controller - is retrieved by a CNN on images taken from a camera. The presence of dynamics and static delay in the steering actuation mechanism and the impossibility to tune the lookahead distance of the PP controller lead to to develop new control strategies in order to guarantee stability, possibly maximizing performance. With the aim of exploiting the already available data, a pure camera based controller that depends only on the input to the PP, is then proposed. Based on the LHE, a proportional gain, a derivative action and a velocity reference generation technique are introduced in order to cope with the missing degrees of freedom on the fixed lookahead distance. A time-delay analysis then proved the advantage introduced by adding these contributions in granting stability at higher speeds and gave an insight on a tuning strategy. Eventually, the results on a test scenario, similar to the one of the challenge, revealed the effectiveness of the proposed control law and allowed to evaluate its tracking performance.
It is worth discussing interesting facts revealed by the results shown in the previous chapter. The proposed PP-based velocity reference generation technique acted well in allowing homogeneity in the motion, thus ensuring robustness. Indeed a major source of limitation of this control action still remains the choice of the fixed lookahead distance with reference to a track with different radii of curvature. In a basic PP scenario the curvature of the road sets a bound on the lookahead distance which has to be selected small enough in order to avoid the "cutting-corner" effect. Decreasing the lookahead distance goes along with the introduction of oscillatory behaviours due to the delay in the control loop and saturations of the control and system variables. In order to compensate for such effect, the derivative contribution acts well in damping oscillations and overshoots at curve exits, thus allowing to increase the velocity along straight sections.
The adopted test scenario didn't allow to increase velocity too much but results applying the proposed lane keeping controller allows to deliver significantly better results than the basic PP controller on a full lap by means of the proposed metrics. A possible further development could be that of embedding this control law in an optimization framework, like in [26], in order to determine the best parameters in a racing scenario.

APPENDIX

A Linearization of LHE output functions

A.1 Circular scenario

In the circular scenario (Fig.2.3), the LLE is well defined as long as $e_{y_c}^2 < L_d^2$ and.takes the form:

$$e_d = e_{y_c} \cos e_\psi + \sqrt{L_d^2 - e_{y_c}^2} \sin e_\psi$$

Given the expression of the circular lateral error (2.12), the inequality $|e_{y_c}| < L_d$ is equivalent to the following system:

$$\begin{cases} \frac{-L_d^2+2(\rho_s-L_d)\, e_y+2\rho_s L_d-L_d^2}{2(\rho_s-e_y)} \geq 0 \\ \frac{-L_d^2+2(\rho_s+L_d)\, e_y-2\rho_s L_d-L_d^2}{2(\rho_s-e_y)} \leq 0 \end{cases}$$

The intervals of existence of the lateral error depend on $L_d \lessgtr \rho_s$ as:

$$e_y \in \begin{cases} [-L_d, 2\rho_s - L_d] & \text{if } L_d \geq \rho_s \\ [-L_d, L_d] & \text{if } L_d < \rho_s \end{cases}$$

The output relation in the circular case can be expressed by:

$$\alpha = \arcsin \frac{e_d}{L_d} = \arcsin \frac{e_{y_c} \cos e_\psi + \sqrt{L_d^2 - e_{y_c}^2} \sin e_\psi}{L_d}$$

$$\frac{\partial \alpha}{\partial e_y} = \frac{1}{\sqrt{1 - \left(\frac{e_d}{L_d}\right)^2}} \frac{1}{L_d} \frac{\partial e_d}{\partial e_y}$$

$$\frac{\partial \alpha}{\partial e_\psi} = \frac{1}{\sqrt{1 - \left(\frac{e_d}{L_d}\right)^2}} \frac{1}{L_d} \frac{\partial e_d}{\partial e_\psi}$$

$$\frac{\partial e_d}{\partial e_y} = \frac{\partial e_{y_c}}{\partial e_y} \cos e_\psi - \frac{e_{y_c}}{\sqrt{L_d^2 - e_{y_c}^2}} \frac{\partial e_{y_c}}{\partial e_y} \sin e_\psi$$

$$\frac{\partial e_d}{\partial e_\psi} = -e_{y_c} \sin e_\psi + \sqrt{L_d^2 - e_{y_c}^2} \cos e_\psi$$

$$\frac{\partial e_{y_c}}{\partial e_y} = \frac{4{\rho_s}^2 + 2e_y^2 - 4\rho_s e_y - 2L_d^2}{4(\rho_s - e_y)^2}$$

A.2 Straight scenario

In the straight path scenario (Fig.2.4), the LLE takes the form:

$$e_d = e_y \cos e_\psi + \sqrt{L_d^2 - e_y^2} \sin e_\psi$$

and therefore it is well defined as long as $e_y^2 < L_d^2$, i.e. $e_y \in [-L_d, L_d]$.
The output relation in the straight case can be expressed by:

$$\alpha = \arcsin \frac{e_d}{L_d} = \arcsin \frac{e_y \cos e_\psi + \sqrt{L_d^2 - e_y^2} \sin e_\psi}{L_d}$$

$$\frac{\partial \alpha}{\partial e_y} = \frac{1}{\sqrt{1 - \left(\frac{e_d}{L_d}\right)^2}} \frac{1}{L_d} \frac{\partial e_d}{\partial e_y}$$

$$\frac{\partial \alpha}{\partial e_\psi} = \frac{1}{\sqrt{1 - \left(\frac{e_d}{L_d}\right)^2}} \frac{1}{L_d} \frac{\partial e_d}{\partial e_\psi}$$

$$\frac{\partial e_d}{\partial e_y} = \cos e_\psi - \frac{e_y}{\sqrt{L_d^2 - e_y^2}} \sin e_\psi$$

$$\frac{\partial e_d}{\partial e_\psi} = -e_y \sin e_\psi + \sqrt{L_d^2 - e_y^2} \cos e_\psi$$

APPENDIX

B Stability analysis of the basic PP controller

In this chapter stability of the basic PP control law (3.3) will be investigated both in the straight and circular scenarios based on [17] by resorting to both a spectral analysis and a Lyapunov based approach.

B.1 Straight scenario

By applying the control law (3.3) to the model (2.7), the following nonlinear state feedback closed loop system is obtained:

$$\dot{\mathbf{x}} = \begin{bmatrix} v \sin e_\psi \\ -\dfrac{2v}{L_d} \sin \alpha \end{bmatrix} = \begin{bmatrix} v \sin e_\psi \\ -\dfrac{2v}{L_d^2} \underbrace{\left(e_y \cos e_\psi + \sqrt{L_d^2 - e_y^2} \sin e_\psi \right)}_{e_d(\mathbf{x})} \end{bmatrix} \tag{B.1}$$

It's easy to verify that the origin $\mathbf{x}_0 = [0, 0]^\top$ is an equilibrium point for the system.

B.1.1 *Stability by linearization*

Stability of a nonlinear system can be checked by computing the eigenvalues of the Jacobian of the system evaluated at the equilibrium point. Taking derivatives of (B.1):

$$J_0 := \begin{bmatrix} \frac{\partial \dot{e}_y}{\partial e_y} & \frac{\partial \dot{e}_y}{\partial e_\psi} \\ \frac{\partial \dot{e}_\psi}{\partial e_y} & \frac{\partial \dot{e}_\psi}{\partial e_\psi} \end{bmatrix} \Bigg|_{\mathbf{x}_0} = \begin{bmatrix} 0 & v \cos e_\psi \\ -\frac{2v}{L_d^2} \left(\cos e_\psi - \frac{e_y}{\sqrt{L_d^2 - e_y^2}} \right) & -\frac{2v}{L_d^2} \left(-e_y \sin e_\psi + \sqrt{L_d^2 - e_y^2} \cos e_\psi \right) \end{bmatrix} \Bigg|_{\mathbf{x}_0}$$

$$= \begin{bmatrix} 0 & v \\ -\dfrac{2v}{L_d^2} & -\dfrac{2v}{L_d} \end{bmatrix}$$

The characteristic polynomial of this matrix is:

$$\det(\lambda I - J_0) = \lambda^2 + \frac{2v}{L_d} \lambda + \frac{2v^2}{L_d^2}$$

whose spectrum is given by the complex conjugate pair:

$$\sigma_{J_0} = \left\{ -\frac{v}{L_d} \pm i \frac{v}{L_d} \right\} \tag{B.2}$$

This implies that the origin of the state space is asymptotically stable for the linear system and therefore also for the nonlinear one.

B.1.2 *Stability by Lyapunov*

The proposed candidate Lyapunov function for the stability of the closed loop system (B.1) is [17]:

$$V(\mathbf{x}) = \frac{1}{2} v^2 \sin^2 e_\psi + \frac{v^2}{L_d^2} e_y^2 \tag{B.3}$$

It can be verified that $V(0,0) = 0$ and $V > 0$ for every $\mathbf{x}$ in the set

$$\mathcal{B}_0 = \left\{ (e_y, e_\psi) \in \mathbb{R} \,\middle|\, \|e_y\| \leq L_d,\ \|e_\psi\| \leq \frac{\pi}{2}, (e_y, e_\psi) \neq (0,0) \right\}$$

The time derivative of V along the trajectories of the system (B.1) can be derived as:

$$\begin{aligned}
\dot{V} &= \frac{\partial V}{\partial e_y} \dot{e}_y + \frac{\partial V}{\partial e_\psi} \dot{e}_\psi \\
&= v^2 \sin e_\psi \cos e_\psi \dot{e}_\psi + \frac{2v^2}{L_d^2} e_y v \sin e_\psi \\
&= v^3 \sin e_\psi \left[\frac{1}{\ell} \tan\delta \cos e_\psi + \frac{2 e_y}{L_d^2} \right] \\
&\overset{\text{PP}}{=} v^3 \sin e_\psi \left[-\frac{2}{L_d} \sin\alpha \cos e_\psi + \frac{2}{L_d} \sin(\alpha - e_\psi) \right] \\
&= -\frac{2v^3}{L_d} \sin^2 e_\psi \cos\alpha
\end{aligned}$$

where the PP control choice (3.3) has been made for δ. If $v > 0$, the derivative of the Lyapunov function is negative semidefinite inside the ball $\mathcal{B}_0$. This is not enough to infer asymptotic stability for the origin but, applying the Barbashin-Krasowskii-LaSalle Invariance Principle, the set containing the trajectories such that $\dot{V} = 0$ contains only the origin $\mathbf{x} = [0,0]^\top$ which is then an asymptotically stable equilibrium point for the closed loop system (B.1). ■

At first glance one might try to exploit geometric intuition, trying to define a Lyapunov function that depends on the LLE. Anyway this is not possible since the LLE does not satisfy the positive definiteness property around the origin, necessary condition for a Lyapunov function: indeed, as plotted in Fig.B.1, the LLE cancels out for states such that

$$e_\psi = \arctan -\frac{e_y}{\sqrt{L_d^2 - e_y^2}} \tag{B.4}$$

These configurations correspond to the car being misplaced laterally and directed towards the lookahead point: in this particular case the LLE (and also the derivative of the heading error) is zero but the car is not on path. An example is shown in Fig.B.2.

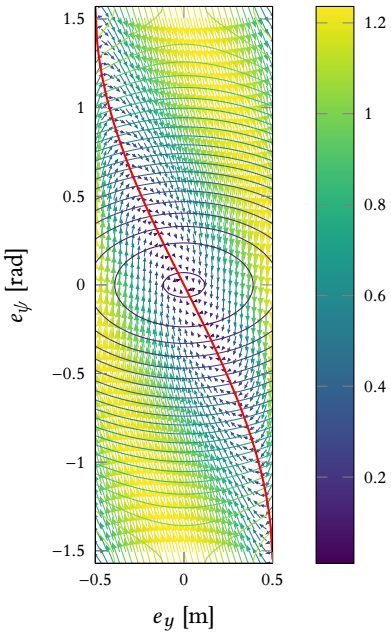

Figure B.1: Vector field of the closed loop control system (B.1) with $L_d = 0.5\,\mathrm{m}$ and $v = 0.3\,\mathrm{m\,s^{-1}}$. The contour lines refer to the Lyapunov function (B.3). The red curve is the locus of points where the derivative of the heading error annihilates as a function of the lateral error

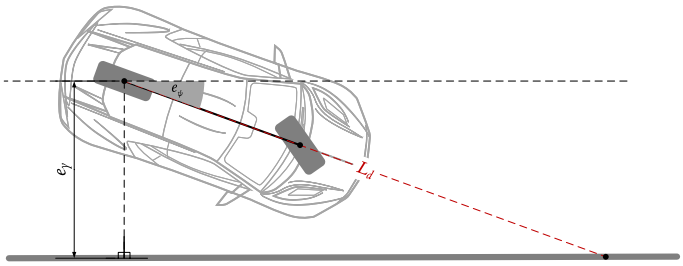

Figure B.2: Configuration in which the LLE e_d annihilates, despite the state being $\mathbf{x} \neq [0, 0]^\top$

B.2 Circular scenario

By applying the control law (3.3) to the model (2.8), the following nonlinear state feedback closed loop system is obtained:

$$\dot{\mathbf{x}} = \begin{bmatrix} v \sin e_\psi \\ -\dfrac{2v}{L_d}\sin\alpha - \dfrac{v\cos e_\psi}{\rho_s - e_y} \end{bmatrix} = \begin{bmatrix} v \sin e_\psi \\ -\dfrac{2v}{L_d^2}\underbrace{\left(e_{y_c}\cos e_\psi + \sqrt{L_d^2 - e_{y_c}^2}\,\sin e_\psi\right)}_{e_d(\mathbf{x})} - \dfrac{v\cos e_\psi}{\rho_s - e_y} \end{bmatrix} \tag{B.5}$$

It is easy to verify that the origin $\mathbf{x}_0 = [0, 0]^\top$ is an equilibrium point for the system.

B.2.1 *Stability by linearization*

The Jacobian of the nonlinear closed loop system evaluated at the equilibrium point $\mathbf{x}_0$ is:

$$\begin{aligned} J_0 &:= \left.\begin{bmatrix} \dfrac{\partial \dot{e}_y}{\partial e_y} & \dfrac{\partial \dot{e}_y}{\partial e_\psi} \\ \dfrac{\partial \dot{e}_\psi}{\partial e_y} & \dfrac{\partial \dot{e}_\psi}{\partial e_\psi} \end{bmatrix}\right|_{\mathbf{x}_0} \\ &= \left.\begin{bmatrix} 0 & v\cos e_\psi \\ -\frac{2v}{L_d^2}\left(\frac{4{\rho_s}^2+2e_y^2-4\rho_s e_y-2L_d^2}{4(\rho_s-e_y)^2}\right) - \frac{v}{(\rho_s-e_y)^2} & -\frac{2v}{L_d^2}\left(-e_{y_c}\sin e_\psi + \sqrt{L_d^2 - e_y^2}\cos e_\psi\right) + \frac{v}{\rho_s-e_y}\sin e_\psi \end{bmatrix}\right|_{\mathbf{x}_0} \\ &= \begin{bmatrix} 0 & v \\ -\dfrac{2v}{L_d^2} & -\dfrac{v}{L_d\rho_s}\sqrt{4{\rho_s}^2 - L_d^2} \end{bmatrix} \end{aligned}$$

The characteristic polynomial of this matrix is:

$$\det(\lambda I - J_0) = \lambda^2 + \frac{v}{L_d\rho_s}\sqrt{4{\rho_s}^2 - L_d^2}\,\lambda + \frac{2v^2}{L_d^2}$$

whose spectrum is given by the pair of complex conjugate eigenvalues:

$$\sigma_{J_0} = \left\{-\frac{v}{2L_d\rho_s}\sqrt{4{\rho_s}^2 - L_d^2} \pm i\,\frac{v}{2L_d\rho_s}\sqrt{4{\rho_s}^2 + L_d^2}\right\} \tag{B.6}$$

This implies that the origin of the state space is asymptotically stable for the linear system and therefore also for the nonlinear one.

B.2.2 *Stability by Lyapunov*

In this case a Lyapunov function is difficult to find but an insight into how to build one can be given on the basis of the work done by Park et al. in [17]. In Fig.B.3 it is represented the vector field of the closed loop system (B.5). It is clear that orbits resemble the ones of a stable focus in the origin. The solid curve represents the locus of points (e_y,e_ψ) where the heading error derivative $\dot{e}_\psi$ annihilates:

$$-v\left[\left(\frac{2e_{y_c}}{L_d^2}+\frac{1}{\rho_s-e_y}\right)\cos e_\psi+\frac{2}{L_d^2}\sqrt{L_d^2-e_{y_c}^2}\sin e_\psi\right]=0 \quad\Longleftrightarrow\quad e_\psi=\arctan-\frac{e_{y_c}+\frac{L_d^2}{2(\rho_s-e_y)}}{\sqrt{L_d^2-e_{y_c}^2}}$$

The dash-dotted curve is the locus of points (e_y,e_ψ) where the lateral error derivative $\dot{e}_y$ annihilates, namely the set $\left\{(e_y,e_\psi)\in\mathbb{R}^2\,\middle|\,e_y\in\mathbb{R},e_\psi=0\right\}$.

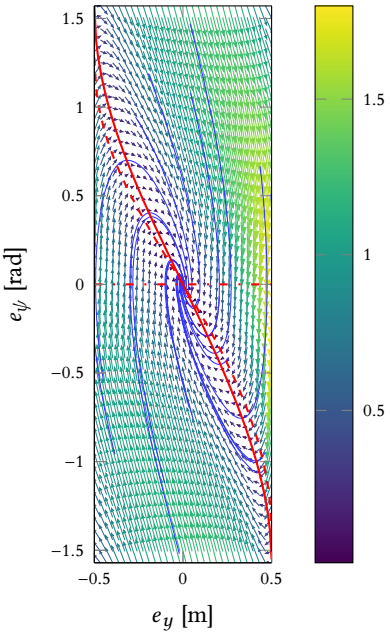

Figure B.3: Vector field of the closed loop control system (B.5) with $L_d = 0.5\,\mathrm{m}$ and $v = 0.3\,\mathrm{m\,s^{-1}}$. The solid, dash-dotted and dashed curves are the locus of points where the derivative of the heading error, the derivative of the lateral error and their sum respectively annihilate as a function of the lateral error.

The dashed curve represents the locus of points (e_y,e_ψ) where their sum annihilates, that is:

$$0=-v\left[\left(\frac{2e_{y_c}}{L_d^2}-\frac{1}{\rho_s-e_y}\right)\cos e_\psi+\left(1+\frac{2}{L_d^2}\sqrt{L_d^2-e_{y_c}^2}\right)\sin e_\psi\right]$$

$$e_\psi = \arctan -\frac{\frac{2e_{y_c}}{L_d^2} - \frac{1}{\rho_s - e_y}}{1 + \frac{2}{L_d^2}\sqrt{L_d^2 - e_{y_c}^2}}$$

These three curves partition the state space into six open sets and, taken together, they impose restrictions on the directions that state trajectories can take in various regions of the state space. Both state derivatives are zero at the stationary point so that it must be an element of all three separation sets. According to [17], a Lyapunov function can then be defined by constructing from every point in the state space a closed polygon obtained by modifying the convergent contour that emanates from that point and crosses the partition lines. Clearly many points will share the same convergent contour and so closed polygons for each contour are constructed, yielding nested polygons. The Lyapunov function at each point in the space can be then defined as the area of the smallest polygon containing that point.

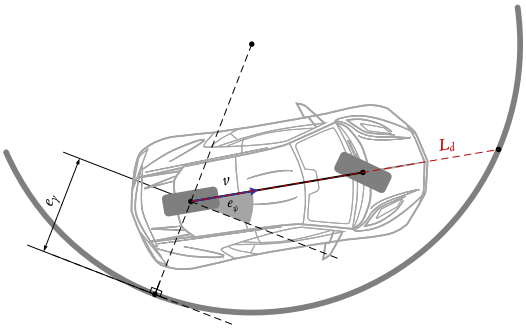

Figure B.4: Configuration in which the LLE e_d annihilates, despite the state being $\mathbf{x} \neq [0, 0]^\top$. In the circular case this is not equivalent to the configurations in which also $\dot{e}_\psi$ annihilates

Bibliography

1. J. Ahn, S. Shin, M. Kim, and J. Park. "Accurate Path Tracking by Adjusting Look-Ahead Point in Pure Pursuit Method". *International Journal of Automotive Technology* 22, 2021, pp. 119–129. DOI: 10.1007/s12239-021-0013-7 (see p. 15).
2. O. Amidi and C. E. Thorpe. "Integrated mobile robot control". In: *Mobile Robots V*. Ed. by W. H. Chun and W. J. Wolfe. Vol. 1388. International Society for Optics and Photonics. SPIE, 1991, pp. 504–523. DOI: 10.1117/12.25494 (see p. 2).
3. M. Buehler, K. Iagnemma, and S. Singh. *The DARPA Urban Challenge: Autonomous Vehicles in City Traffic*. 1st. Springer Publishing Company, Incorporated, 2009 (see p. 2).
4. S. F. Campbell. "Steering control of an autonomous ground vehicle with application to the DARPA Urban Challenge". In: 2007 (see p. 2).
5. R. C. Coulter. *Implementation of the Pure Pursuit Path Tracking Algorithm*. Tech. rep. CMU-RI-TR-92-01. Pittsburgh, PA: Carnegie Mellon University, 1992 (see p. 2).
6. A. De Luca, G. Oriolo, and C. Samson. "Feedback control of a nonholonomic car-like robot". In: *Robot Motion Planning and Control*. Ed. by J. P. Laumond. Springer Berlin Heidelberg, Berlin, Heidelberg, 1998, pp. 171–253. DOI: 10.1007/BFb0036073 (see pp. 6–8).
7. C. M. Filho, D. F. Wolf, V. Grassi, and F. S. Osório. "Longitudinal and lateral control for autonomous ground vehicles". In: *2014 IEEE Intelligent Vehicles Symposium Proceedings*. 2014, pp. 588–593. DOI: 10.1109/IVS.2014.6856431 (see pp. 2, 24).
8. Y. Gao, A. Gray, J. V. Frasch, T. Lin, E. Tseng, J. K. Hedrick, and F. Borrelli. "Spatial Predictive Control for Agile Semi-Autonomous Ground Vehicles". In: 2012 (see p. 7).
9. R. Jazar. *Vehicle Dynamics: Theory and Application*. 2008 Springer E-Books. Springer US, 2008 (see p. 6).
10. J. Kong, M. Pfeiffer, G. Schildbach, and F. Borrelli. "Kinematic and dynamic vehicle models for autonomous driving control design". In: *2015 IEEE Intelligent Vehicles Symposium (IV)*. 2015, pp. 1094–1099. DOI: 10.1109/IVS.2015.7225830 (see p. 7).
11. C. A. Molnar, T. Balogh, I. Boussaada, and T. Insperger. "Calculation of the critical delay for the double inverted pendulum". *Journal of Vibration and Control* 27:3-4, 2021, pp. 356–364. DOI: 10.1177/1077546320926909. eprint: https://doi.org/10.1177/1077546320926909 (see p. 28).

12. S. Moveh, H. Mohamed, and M. Maziah Binti. "Article: A Review of some Pure-Pursuit based Path Tracking Techniques for Control of Autonomous Vehicle". *International Journal of Computer Applications* 135:1, 2016. Published by Foundation of Computer Science (FCS), NY, USA, pp. 35–38 (see p. 2).
13. K. Murphy. "Analysis of Robotic Vehicle Steering and Controller Delay". en. In: To be presented at the 5th International Symposium on Robotics and Manufacturing, Maui, HI, 1994 (see pp. 2, 17).
14. A. Ollero and G. Heredia. "Stability analysis of mobile robot path tracking". In: *Proceedings 1995 IEEE/RSJ International Conference on Intelligent Robots and Systems. Human Robot Interaction and Cooperative Robots*. Vol. 3. 1995, 461–466 vol.3. DOI: 10.1109/IROS.1995.525925 (see pp. 2, 9, 29).
15. B. Paden, M. Cap, S. Z. Yong, D. Yershov, and E. Frazzoli. *A Survey of Motion Planning and Control Techniques for Self-driving Urban Vehicles*. 2016. DOI: 10.48550/ARXIV.1604.07446 (see pp. 2, 7, 8).
16. S. Park, J. Deyst, and J. P. How. "A new nonlinear guidance logic for trajectory tracking". In: *In Proceedings of the AIAA Guidance, Navigation and Control Conference*. 2004, pp. 2004–4900 (see pp. 16, 24).
17. S. Park, J. Deyst, and J. P. How. "Performance and Lyapunov Stability of a Nonlinear Path Following Guidance Method". *Journal of Guidance, Control, and Dynamics* 30:6, 2007, pp. 1718–1728. DOI: 10.2514/1.28957. eprint: https://doi.org/10.2514/1.28957 (see pp. 2, 14, 53, 54, 57, 58).
18. "Preliminary Results for Analyzing Systems with Time Delay". In: *PID Controllers for Time-Delay Systems*. Birkhäuser Boston, Boston, MA, 2005, pp. 77–107. DOI: 10.1007/0-8176-4423-7_5 (see p. 27).
19. M. Rokonuzzaman, N. Mohajer, S. Nahavandi, and S. Mohamed. "Review and performance evaluation of path tracking controllers of autonomous vehicles". *IET Intelligent Transport Systems* 15:5, 2021, pp. 646–670. DOI: https://doi.org/10.1049/itr2.12051. eprint: https://ietresearch.onlinelibrary.wiley.com/doi/pdf/10.1049/itr2.12051 (see pp. 2, 45).
20. L. L. Scharf, W. P. Harthill, and P. H. Moose. "A comparison of expected flight times for intercept and pure pursuit missiles". *IEEE Transactions on Aerospace and Electronic Systems* AES-5:4, 1969, pp. 672–673. DOI: 10.1109/TAES.1969.309951 (see p. 2).
21. J. M. Snider. *Automatic Steering Methods for Autonomous Automobile Path Tracking*. Tech. rep. CMU-RI-TR-09-08. Pittsburgh, PA: Carnegie Mellon University, 2009 (see p. 15).
22. V. Sukhil and M. Behl. "Adaptive Lookahead Pure-Pursuit for Autonomous Racing". *CoRR* abs/2111.08873, 2021. arXiv: 2111.08873 (see p. 15).
23. L. H. Vy Nguyen, C. Bonnet, I. Boussaada, and M. Souaiby. "A problematic issue in the Walton-Marshall method for some neutral delay systems". In: *2019 IEEE 58th Conference on Decision and Control (CDC)*. 2019, pp. 971–975. DOI: 10.1109/CDC40024.2019.9030182 (see p. 28).

24. R. Wallace, A. Stentz, C. Thorpe, H. Maravec, W. Whittaker, and T. Kanade. "First Results in Robot Road-Following". In: *Proceedings of the 9th International Joint Conference on Artificial Intelligence - Volume 2*. IJCAI'85. Morgan Kaufmann Publishers Inc., Los Angeles, California, 1985, pp. 1089–1095 (see p. 2).

25. K. Walton and J. Marshall. "Direct method for TDS stability analysis". English. *IEE Proceedings D (Control Theory and Applications)* 134, 2 1987, 101–107(6) (see p. 27).

26. L. Wang, Z. Chen, and W. Zhu. "An improved pure pursuit path tracking control method based on heading error rate". *Industrial Robot: the international journal of robotics research and application* 49:5, 2022, pp. 973–980. DOI: 10.1108/IR-11-2021-0257 (see pp. 2, 49).

27. S. Xu, H. Peng, and Y. Tang. "Preview Path Tracking Control With Delay Compensation for Autonomous Vehicles". *IEEE Transactions on Intelligent Transportation Systems* 22:5, 2021, pp. 2979–2989. DOI: 10.1109/TITS.2020.2978417 (see p. 12).

28. Q. Yao, Y. Tian, Q. Wang, and S. Wang. "Control Strategies on Path Tracking for Autonomous Vehicle: State of the Art and Future Challenges". *IEEE Access* 8, 2020, pp. 161211–161222. DOI: 10.1109/ACCESS.2020.3020075 (see p. 2).